Journal of Medicinal Chemistry

Article

pubs.acs.org/jmc

Synthesis and Anticancer Mechanism Investigation of Dual Hsp27 and Tubulin Inhibitors

Bo Zhong,[†] Snigdha Chennamaneni,[†] Rati Lama,[†] Xin Yi,[†] Werner J. Geldenhuys,[§] John J. Pink,[∥] Afshin Dowlati,[⊥] Yan Xu,[†] Aimin Zhou,[†,‡] and Bin Su*[,†,‡]

[†]Department of Chemistry, College of Sciences and Health Professions, Cleveland State University, 2121 Euclid Avenue, Cleveland, Ohio 44115, United States

[‡]Center for Gene Regulation in Health and Disease, College of Sciences and Health Professions, Cleveland State University, 2121 Euclid Avenue, Cleveland, Ohio 44115, United States

[§]Department of Pharmaceutical Sciences, Northeast Ohio Medical University, 4209 State Route 44, Rootstown, Ohio 44272, United States

[∥]Division of General Medical Sciences—Oncology, Case Western Reserve University School of Medicine, 10900 Euclid Avenue, Cleveland, Ohio 44106, United States

[⊥]Division of Hematology and Oncology, Case Western Reserve University School of Medicine, 10900 Euclid Avenue, Cleveland, Ohio 44106, United States

S *Supporting Information*

ABSTRACT: Heat shock protein 27 (Hsp27) is a chaperone protein, and its expression is increased in response to various stress stimuli including anticancer chemotherapy, which allows the cells to survive and causes drug resistance. We previously identified lead compounds that bound to Hsp27 and tubulin via proteomic approaches. Systematic ligand based optimization in the current study significantly increased the cell growth inhibition and apoptosis inducing activities of the compounds. Compared to the lead compounds, one of the new derivatives exhibited much better potency to inhibit tubulin polymerization but a decreased activity to inhibit Hsp27 chaperone function, suggesting that the structural modification dissected the dual targeting effects of the compound. The most potent compounds **20** and **22** exhibited strong cell proliferation inhibitory activities at subnanomolar concentration against 60 human cancer cell lines conducted by Developmental Therapeutic Program at the National Cancer Institute and represented promising candidates for anticancer drug development.

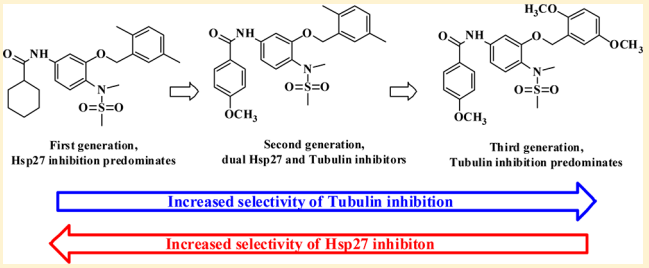

1. INTRODUCTION

The expression of heat shock proteins (Hsp) is increased under lethal conditions, which is a typical response when cancer cells are stressed by chemotherapies.[1−3] Hsp27, a small heat shock protein, shows a very tight correlation with anticancer drug resistance.[3,4] Its overexpression enhances the survival of mammalian cells exposed to anticancer agents.[5] The Hsp27 protective effects come from its molecular chaperone functions at multiple control points of the apoptotic pathways to eliminate anticancer agents induced programmed cell death.[6−8] Hsp27 negatively regulates the activation of pro-caspase 9 via interaction with cytochrome *c* and therefore blocks the formation of the apoptosome complex.[7−9] In addition, Hsp27 can inhibit caspase 3 activity via direct interaction with the pro-caspase 3 molecule.[10] Other evidence has demonstrated that a significant pool of Hsp27 is located in the mitochondrial fraction of thermotolerant Jurkat cells, where it functions against apoptotic stimuli by blocking the release of cytochrome *c*.[11] Overall, Hsp27 has strong antiapoptotic properties and functions at multiple steps of the apoptotic signaling pathway.

Mammalian Hsp27 has a molecular weight of 27 kDa; however, it can form oligomeric complexes in the range 100 ± 800 kDa.[9,12,13] The oligomerization of Hsp27 is a highly dynamic process that depends on the physiology of the cells, phosphorylation status of the protein, and exposure to stress.[5,6,14] It has been well investigated that large oligomers of Hsp27 are required for the chaperone activity, and the oligomers protect cells from oxidative stress, whereas this activity is down-regulated by phosphorylation-driven dissociation of the large oligomers.[6,9]Preventing the formation of Hsp27 large oligomers can decrease the chaperone activity and promote cell apoptosis, which has been demonstrated by the investigation on some small molecules.[15] Up-regulated expression of Hsp27 leads to an overactive chaperone activity, which in turn contributes to the anticancer drug resistance.[1,2]

Received: January 28, 2013
Published: June 16, 2013

Clinically, increased level of Hsp27 in a number of cancers such as breast cancer, endometrial cancer, and leukemia has been detected.[1,2,16−20] The fact that Hsp27 is often highly expressed in cells or tissues from a wide range of tumors supports the hypothesis that this protein could limit the efficacy of cancer therapy. It will be highly desirable to target Hsp27 as cancer therapy. Hsp27 modulators can decrease the protective function of the protein in cell apoptotic regulation.[4,21,22] These agents exhibit promising antitumor activities in preclinical models of a variety of tumors expressing high levels of Hsp27 and may have significant clinical potential.[16,21,22]

So far, the most effective strategy to target Hsp27 is antisense oligonucleotides (ASO) or siRNA, which can decrease Hsp27 expression in in vitro cell culture and in vivo xenograft as well.[4,22] The fourth generation ASO of Hsp27, OGX-427,[16] has shown clinical evidence of antitumor activity despite the limitations associated with ASO administration. The results further underline that Hsp27 is a good anticancer target. Small molecule Hsp27 modulators without the administration problems are highly possible to show even better clinical outcomes. The difficulties of developing small molecule Hsp27 inhibitors include three critical factors: (1) Hsp27 does not have endogenous ligand, and there is no information about the binding site of the protein; (2) the dynamic oligomeric process of Hsp27 is correlated to its function, and this dynamic characteristic makes it difficult to evaluate small molecules binding to Hsp27; (3) there is an absence of clearly demonstrated Hsp27 pathway downstream proteins that are directly affected by Hsp27 inhibitors. Therefore, it is difficult to define a cellular biomarker for these small molecules.

Through biotinylated small molecular probe, affinity chromatography, and proteomic approaches, we previously identified potent anticancer agents that are dual ligands binding to Hsp27 and tubulin.[23,24] Systematic ligand based optimization in the current study dramatically increased the cell proliferation inhibition and apoptosis inducing activities of the compounds. The preliminary mechanism study suggests that tubulin inhibitory efficacy of the new derivatives was significantly improved, and the inhibition of the Hsp27 chaperone activity was decreased on one of the analogues. It seems that the structural modification dissected the two activities. Some of the new analogues became more potent and selective tubulin inhibitors. The structure−activity relationship (SAR) summarized from the study provided us with a foundation to further dissect the two activities and develop pure Hsp27 or tubulin inhibitors.

2. RESULTS AND DISCUSSIONS

2.1. Lead Optimization and Summarization of the SAR. Our previous efforts to develop the potent anticancer agents led to the discovery of compound **48** (NSC751382,[25] Figure 1), benzo[1,3]dioxole-5-carboxylic acid [3-(2,5-dimethylbenzyloxy)-4-(methanesulfonylmethylamino)phenyl]amide, which displayed potent antiproliferative activity against various cancer cell lines with IC_{50} values in the range of 0.1−0.5 μM. The molecular targets of this compound were subsequently identified to be Hsp27 and tubulin.[24] In the present study, a total of 42 new derivatives based on compound **48** were synthesized using combinatory strategy. First, we kept C and D moieties as *N*-methyl methylsulfonamide, and changed A and B moieties systematically (Table 1). Previous SAR study of A and B moieties revealed that 2,5-dimethylbenzyl and 2,5-dichlorobenzyl-substituted B position led to more active compounds.[25,26] In the newly designed derivatives, we explored other 2,5-disubstituted benzyl groups including 2,5-dimethoxybenzyl and 2-methyl-5-trifluoromethylbenzyl. Additionally, *n*-hexyl group at the B position was also evaluated in order to determine if the hydrophobic and flexible alkyl chain could be well accommodated. Moiety A was modified to six substituted aryl groups including 4-bromophenyl, 4-methoxyphenyl, 3,4-dimethylphenyl, 4-iodophenyl, 2-naphthyl, and 3,4-methylenedioxyphenyl. These six substituted aryl groups were previously demonstrated to be the best fit while keeping B position as 2,5-dimethylbenzyl and C position as methylsulfonamide and D position as methyl group.[25] We anticipated that the new combination of A and B moieties would generate more active compounds. Additionally, the alternative to methylsulfonamide at C position was investigated by substitution with the trifluoromethylsulfonamide group. In drug design, the trifluoromethyl group is often used as a bioisostere to replace the methyl group in drug candidates for improved pharmacological activity. Trifluoromethyl is a very strong electron-withdrawing group and can form strong interactions with target protein through hydrogen bonds or polar contact. It is interesting to know whether a trifluoromethylsulfonamide group in place of the methylsulfonamide group or a trifluoromethyl group in place of the methyl group of the benzyl moiety can improve the molecular binding to target proteins and thereby increase the biological activities.

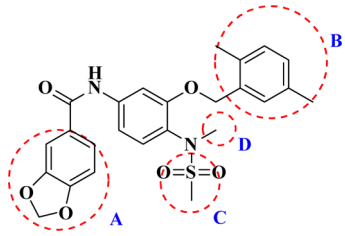

Figure 1. Structure of compound **48**.

Methanesulfonamide derivatives **1**−**30** were prepared according to the published method (Scheme 1).[25] The alkylation of the hydroxyl group of 2-amino-5-nitrophenol was followed by mesylation of the amino group by methanesulfonyl chloride and sodium hydroxide mediated hydrolysis of *N*,*N*-bismethanesulfonamide to afford the monomethanesulfonamide intermediate. This intermediate either underwent N-methylation of the sulfonamide group, reduction of the nitro group, and then amidation of amino group to yield compounds **1**−**24** or was directly subjected to reduction and amidation to give compounds **25**−**30**. Our first attempt to react O-alkylated 2-amino-5-nitrophenol with trifluoromethylsulfonyl chloride in the presence of sodium hydride in dry *N*,*N*-dimethylformamide (DMF) failed to yield trifluoromethanesulfonamide. So more reactive trifluoromethanesulfonic anhydride was used instead and DMF was replaced with diethyl ether as solvent, since DMF is incompatible with trifluoromethanesulfonic anhydride. The obtained trifluoromethanesulfonamide intermediate was subsequently subjected to methylation, reduction, and amidation to yield the expected compounds **31**−**42**.

All the compounds were evaluated for the inhibition of SKBR-3 breast cancer cell proliferation, and the results are summarized in Tables 1 and 2. The IC_{50} values of lead compound **48** and several previously synthesized 2,5-dimethylbenzyl analogues assigned as compounds **43**−**49** are

dx.doi.org/10.1021/jm4004736 | J. Med. Chem. 2013, 56, 5306−5320

Table 1. SAR of A and B Moiety Methanesulfonamide

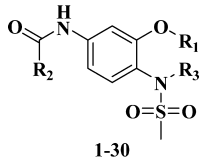

1-30

Entry	R_1	R_2	R_3	IC_{50}
1	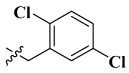	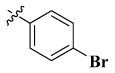	CH_3	2.29 ± 1.09 μM
2	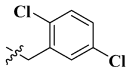	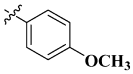	CH_3	0.49 ± 0.28 μM
3	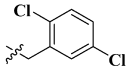	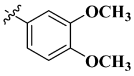	CH_3	3.73 ± 1.81 μM
4	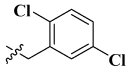	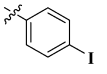	CH_3	0.66 ± 0.31 μM
5	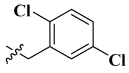	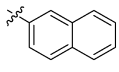	CH_3	2.21 ± 0.98 μM
6	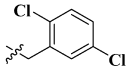	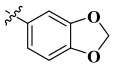	CH_3	2.85 ± 1.48 μM
7	n-C_6H_{13}	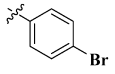	CH_3	39.91 ± 16.24 μM
8	n-C_6H_{13}	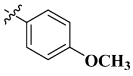	CH_3	19.98 ± 10.51 μM
9	n-C_6H_{13}	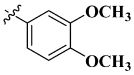	CH_3	100.41 ± 53.14 μM
10	n-C_6H_{13}	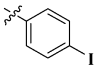	CH_3	12.66 ± 7.48 μM
11	n-C_6H_{13}	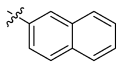	CH_3	64.31 ± 44.71 μM
12	n-C_6H_{13}	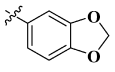	CH_3	28.76 ± 16.98 μM
13	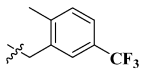	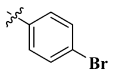	CH_3	9.49 ± 5.02 μM
14	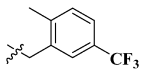	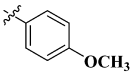	CH_3	2.03 ± 1.35 μM
15	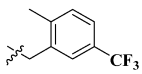	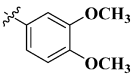	CH_3	16.94 ± 14.51 μM
16	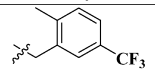	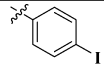	CH_3	3.50 ± 2.06 μM
17	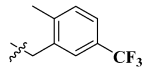	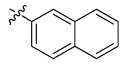	CH_3	18.40 ± 15.28 μM
18	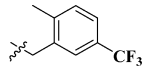	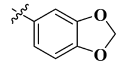	CH_3	14.72 ± 8.37 μM
19	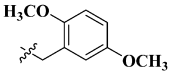	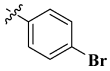	CH_3	3.51 ± 1.91 nM
20	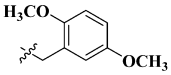	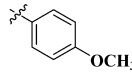	CH_3	2.56 ± 0.37 nM
21	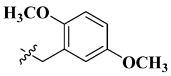	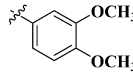	CH_3	2.61 ± 1.31 nM
22	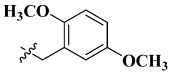	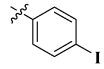	CH_3	1.21 ± 0.71 nM
23	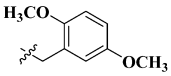		CH_3	16.61 ± 7.71 nM
24			CH_3	7.52 ± 2.81 nM
25			H	9.58 ± 4.23 nM
26			H	13.40 ± 7.13 nM
27			H	11.0 ± 4.45 nM
28			H	11.83 ± 4.78 nM
29			H	13.27 ± 7.11 nM
30			H	35.25 ± 21.74 nM

listed in Table 3 for comparison.[25,27] The results suggest that the B moiety is critical for the antiproliferative activity of this series of compounds (Table 1). The general order of potency is 2,5-dimethoxybenzyl derivatives ≫ 2,5-dimethylbenzyl derivatives > 2,5-dichlorobenzyl derivatives > 2-methyl-5-trifluoromethylbenzyl derivatives > *n*-hexyl derivatives. The electron-donating groups on the 2,5-positions of the benzyl ring seemed to be beneficial for the biological activity. Flexible alkyl chain replacing benzyl moiety dramatically decreased the activity, suggesting that the benzyl moiety is critical for the activity. Additionally, 4-methoxybenzamide and 4-iodobenzamide analogues showed better inhibition potency than the other four amide derivatives including 4-bromobenzamide, 3,4-dimethoxybenzamide, 2-naphthylamide, and 3,4-methylenedioxybenzamide. This new combination of A and B moieties generated several potent compounds **19**−**24** with IC_{50} values at subnanomolar concentrations. Further SAR study of C and D moieties revealed the importance of the methyl group and methylsulfonylamide at the C and D positions, respectively. Removal of the *N*-methyl group in compounds **19**−**22** and **24** to afford **25**−**28** and **30** resulted in 3- to 10-fold loss in inhibitory potency, with the exception that compound **29** showed slightly better potency than **23**. The trifluoromethylsulfonamide group replacing the methylsulfonamide group significantly impaired the cell proliferation inhibitory activity as shown in Table 2. In the case of 2,5-dimethylbenzyl derivatives, trifluoromethylsulfonamides **37**−**42** exhibited 35- to 207-fold lower potency than the corresponding methylsulfonamides **43**−**48**. Similarly for 2,5-dimethoxybenzyl derivatives, trifluoro-

dx.doi.org/10.1021/jm4004736 | *J. Med. Chem.* 2013, 56, 5306−5320

Scheme 1. Synthesis of Compounds 1−42[a]

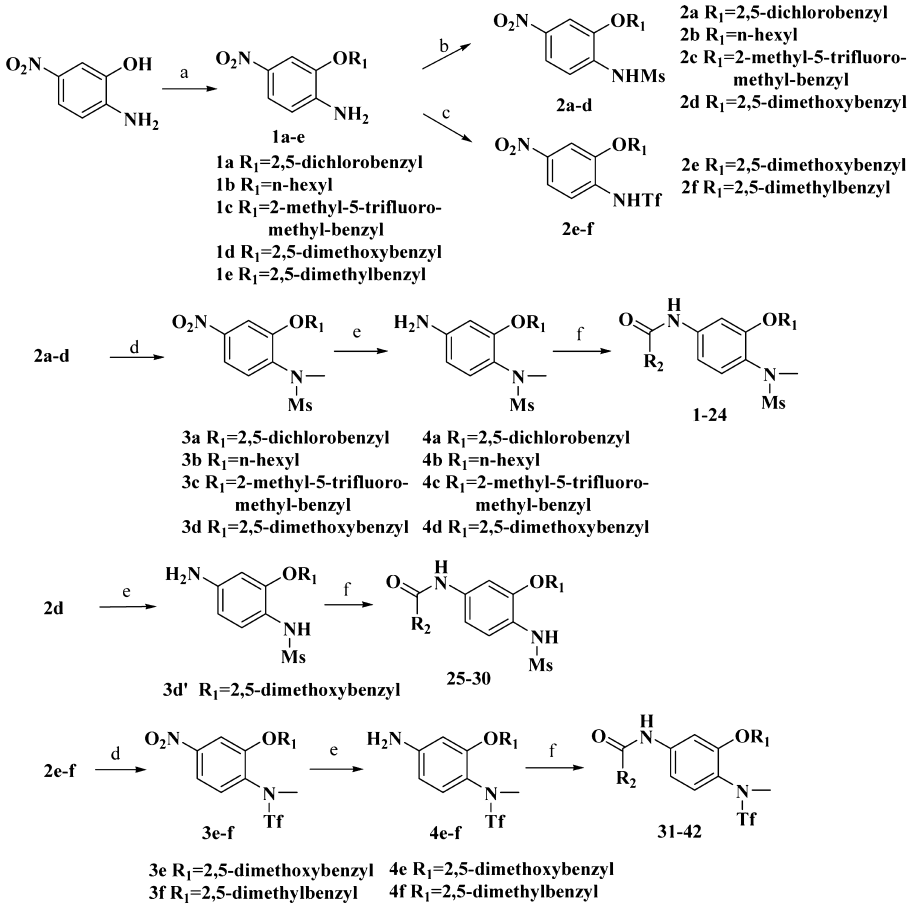

1 R_1=2,5-dichlorobenzyl; R_2=4-bromophenyl
2 R_1=2,5-dichlorobenzyl; R_2=4-methoxyphenyl
3 R_1=2,5-dichlorobenzyl; R_2=3,4-dimethoxyphenyl
4 R_1=2,5-dichlorobenzyl; R_2=4-Iodophenyl
5 R_1=2,5-dichlorobenzyl; R_2=2-naphthyl
6 R_1=2,5-dichlorobenzyl; R_2=3,4-methylenedioxyphenyl
7 R_1=n-hexyl; R_2=4-bromophenyl
8 R_1=n-hexyl; R_2=4-methoxyphenyl
9 R_1=n-hexyl; R_2=3,4-dimethoxyphenyl
10 R_1=n-hexyl; R_2=4-Iodophenyl
11 R_1=n-hexyl; R_2=2-naphthyl
12 R_1=n-hexyl; R_2=3,4-methylenedioxyphenyl
13 R_1=2-methyl-5-trifluoromethyl-benzyl; R_2=4-bromophenyl
14 R_1=2-methyl-5-trifluoromethyl-benzyl; R_2=4-methoxyphenyl
15 R_1=2-methyl-5-trifluoromethyl-benzyl; R_2=3,4-dimethoxyphenyl
16 R_1=2-methyl-5-trifluoromethyl-benzyl; R_2=4-Iodophenyl
17 R_1=2-methyl-5-trifluoromethyl-benzyl; R_2=2-naphthyl
18 R_1=2-methyl-5-trifluoromethyl-benzyl; R_2=3,4-methylenedioxyphenyl
19 R_1=2,5-dimethoxybenzyl; R_2=4-bromophenyl
20 R_1=2,5-dimethoxybenzyl; R_2=4-methoxyphenyl
21 R_1=2,5-dimethoxybenzyl; R_2=3,4-dimethoxyphenyl
22 R_1=2,5-dimethoxybenzyl; R_2=4-Iodophenyl
23 R_1=2,5-dimethoxybenzyl;R_2=2-naphthyl
24 R_1=2,5-dimethoxybenzyl; R_2=3,4- methylenedioxyphenyl
25 R_1=2,5-dimethoxybenzyl; R_2=4-bromophenyl
26 R_1=2,5-dimethoxybenzyl; R_2=4-methoxyphenyl
27 R_1=2,5-dimethoxybenzyl; R_2=3,4-dimethoxyphenyl
28 R_1=2,5-dimethoxybenzyl; R_2=4-Iodophenyl
29 R_1=2,5-dimethoxybenzyl;R_2=2-naphthyl
30 R_1=2,5-dimethoxybenzyl; R_2=3,4-methylenedioxyphenyl
31 R_1=2,5-dimethoxybenzyl; R_2=4-bromophenyl
32 R_1=2,5-dimethoxybenzyl; R_2=4-methoxyphenyl
33 R_1=2,5-dimethoxybenzyl; R_2=3,4-dimethoxyphenyl
34 R_1=2,5-dimethoxybenzyl; R_2=4-Iodophenyl
35 R_1=2,5-dimethoxybenzyl;R_2=2-naphthyl
36 R_1=2,5-dimethoxybenzyl; R_2=3,4-methylenedioxyphenyl
37 R_1=2,5-dimethylbenzyl; R_2=4-bromophenyl
38 R_1=2,5-dimethylbenzyl; R_2=4-methoxyphenyl
39 R_1=2,5-dimethylbenzyl; R_2=3,4-dimethoxyphenyl
40 R_1=2,5-dimethylbenzyl; R_2=4-Iodophenyl
41 R_1=2,5-dimethylbenzyl;R_2=2-naphthyl
42 R_1=2,5-dimethylbenzyl; R_2=3,4-methylenedioxyphenyl

[a]Reagents and conditions: (a) R_1X, DMF, X = Cl, Br, or I; (b) (1) MsCl, NaH, DMF, (2) NaOH, MeOH; (c) Tf_2O, NaH, Et_2O; (d) MeI, NaH, DMF; (e) $FeCl_3$, Zn, DMF/H_2O; (f) R_2COCl, K_2CO_3, 1,4-dioxane.

methyl sulfonamides **31−36** are 12- to 282-fold less potent than the corresponding methyl sulfonamides **19**-**24**.

2.2. Cell Cycle Studies. The lead compound **48** was identified to be dual Hsp27 and tubulin binder[24] and exhibited significant cell cycle arrest activity in our previous studies.[25] Some of the newly generated derivatives such as **19−24** displayed significantly improved cytotoxicity. It is necessary to determine if the new potent derivatives still retain the antimitotic activity of the lead compound, which is characterized by G_2/M phase cell accumulation.[25] Two representative compounds **20** and **22** were examined to elucidate the anticancer mechanism. Both compounds inhibited SKBR-3

dx.doi.org/10.1021/jm4004736 | J. Med. Chem. 2013, 56, 5306−5320

Table 2. SAR of A and B Moiety Trifluoromethylsulfonamides

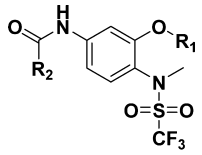

31-42

Entry	R_1	R_2	IC_{50}
31	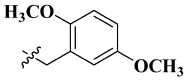	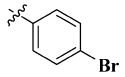	0.47 ± 0.21 μM
32	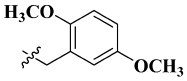	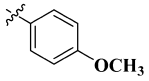	0.11 ± 0.06 μM
33	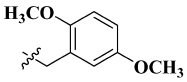	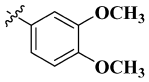	0.55 ± 0.23 μM
34	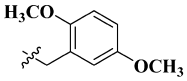	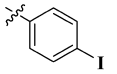	0.51 ± 0.22 μM
35	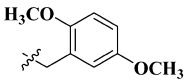	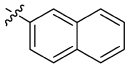	0.20 ± 0.09 μM
36	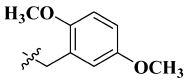	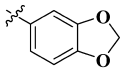	0.71 ± 0.32 μM
37	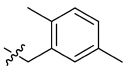	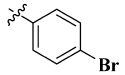	36.44 ± 28.86 μM
38	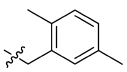	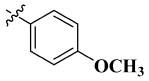	5.32 ± 3.85 μM
39	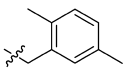	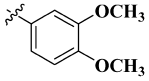	39.28 ± 35.11 μM
40	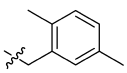	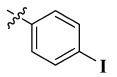	13.49 ± 9.27 μM
41	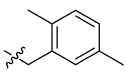	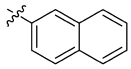	41.40 ± 34.54 μM
42	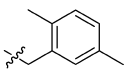	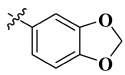	21.78 ± 16.07 μM

Table 3. Previous Developed Dual Hsp27 and Tubulin Binders

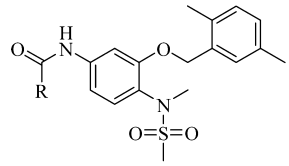

43-50

entry	R	IC_{50}
43	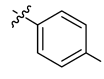	0.22 ± 0.01 μM
44	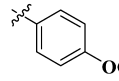	0.15 ± 0.05 μM
45	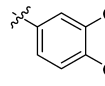	0.19 ± 0.14 μM
46		0.13 ± 0.07 μM
47		0.21 ± 0.01 μM
48	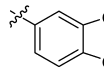	0.20 ± 0.01 μM
49		3.17 ± 1.45 μM

Table 4. Summary of Altered Cell Cycle Distribution in Response to Treatment with 20 and 22[a]

concn	sub-G1 (%)	G1 (%)	S (%)	G2/M (%)
DMSO	3.23	69.63	16.34	10.77
1.0 nM **20**	17.10	61.21	8.71	12.78
2.5 nM **20**	27.43	34.91	8.92	28.57
5.0 nM **20**	33.54	32.02	8.83	25.47
1.0 nM **22**	14.73	66.68	8.45	9.24
2.5 nM **22**	22.02	60.08	9.49	8.10
5.0 nM **22**	24.27	51.84	9.51	13.76
50.0 nM **22**	32.88	31.22	11.39	24.32

[a]SKBR-3 cells were treated for 24 h with the indicated concentrations of compounds. Cells were processed for FACS using propidium iodide staining as described. The percent distribution of cells in each cell cycle phase is displayed.

cell proliferation with IC_{50} of around 2 nM. When the cells were treated with 1 nM of the two compounds, a significant amount of cells were halted at sub-G_1 phase after 24 h, suggesting cell apoptosis. When the dosage was increased to 2.5 and 5 nM for compound **20**, cells started to accumulate at G_2/M phase as well as sub-G_1 phase after 24 h (Table 4). However, for compound **22**, 2.5 and 5 nM treatment clearly induced sub-G_1 phase cell accumulation after 24 h, but a significant G_2/M phase cell accumulation was only observed at 50 nM. The results suggest that compounds **20** and **22** displayed different antimitotic potency, and compound **20** is possibly more active to target tubulin. Apparently, the structural optimization improved the antimitotic effect of the lead compound **48** that affected the cell cycle at 200 nM.[25] Particularly, compound **20** showed cell cycle arrest activity at a concentration as low as 2.5 nM. In addition, both compounds at subnanomolar concentrations clearly induced sub-G_1 phase cell accumulation, suggesting that both compounds exhibited potent cell apoptosis inducing activity. To confirm this effect, we checked caspase 3 and its downstream protein poly ADP-ribose polymerase (PARP) after the treatment with the two compounds. The protein levels of cleaved caspase 3, and cleaved PARP were remarkably increased after a 24 h treatment of SKBR-3 cells with compounds **20** and **22** (Figure 2). The results indicate that these small molecules can promote caspase 3 activation and thereby induce cell apoptosis.

2.3. Inhibition of Tubulin Polymerization. Lead compound **48** in a previous study inhibited tubulin polymerization in the enzyme and live-cell assays.[24] Compared to compound **48** and several previously synthesized analogues, the new derivatives **20** and **22** in this study displayed much more

dx.doi.org/10.1021/jm4004736 | J. Med. Chem. 2013, 56, 5306−5320

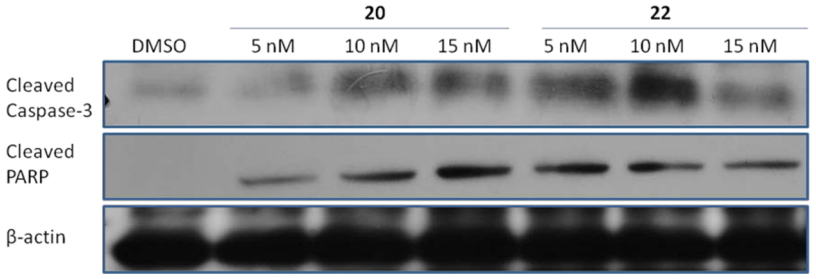

Figure 2. Compounds **20** and **22** induced SKBR-3 cell apoptosis. SKBR-3 cells were treated with DMSO and compounds **20** and **22** for 24 h. Apoptosis was characterized by Western blot analysis of cleaved caspase 3 and cleaved PARP as described in Experimental Section.

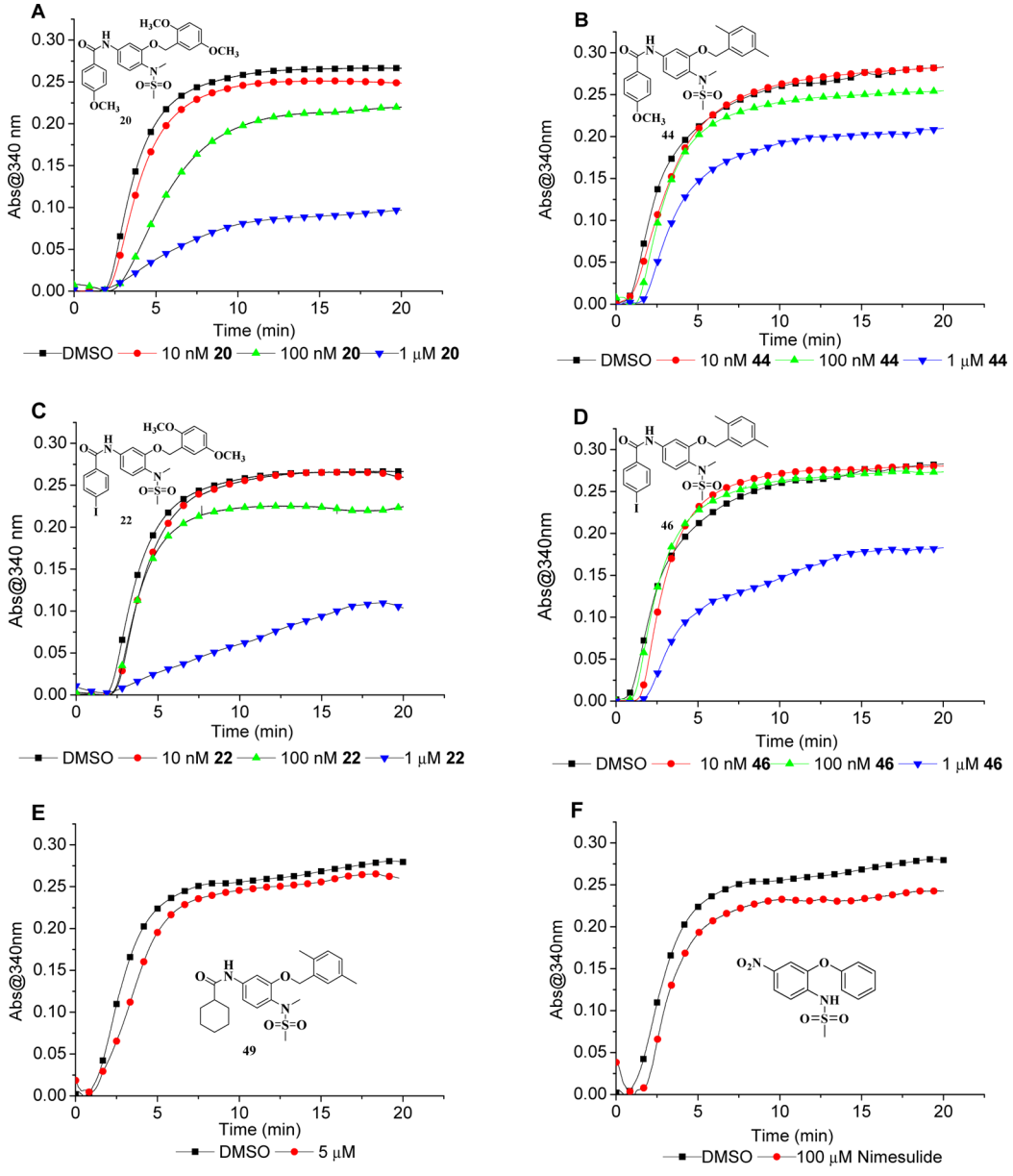

Figure 3. Tubulin polymerization in the presence of different concentrations of compounds **20**, **22**, **44**, **46**, **49** and nimesulide.

potent antimitotic activity in subnanomolar concentrations. We wonder if the cell cycle arrest activity is correlated with the tubulin polymerization inhibitory potency. Therefore, compounds **20** and **22** as well as their respective structural analogues **44** and **46** were examined with the tubulin polymerization assay to analyze the correlation. As shown in Figure 3, all four compounds inhibited tubulin polymerization in a dose dependent manner. In 15 min, compound **44** inhibited tubulin polymerization by 8% at 100 nM and 25% at 1 μM. Compared to **44**, compound **20** displayed more potent tubulin polymerization inhibition by 5% at 10 nM, 19% at 100 nM, and 66% at 1 μM. Compound **22** showed improved

dx.doi.org/10.1021/jm4004736 | J. Med. Chem. 2013, 56, 5306−5320

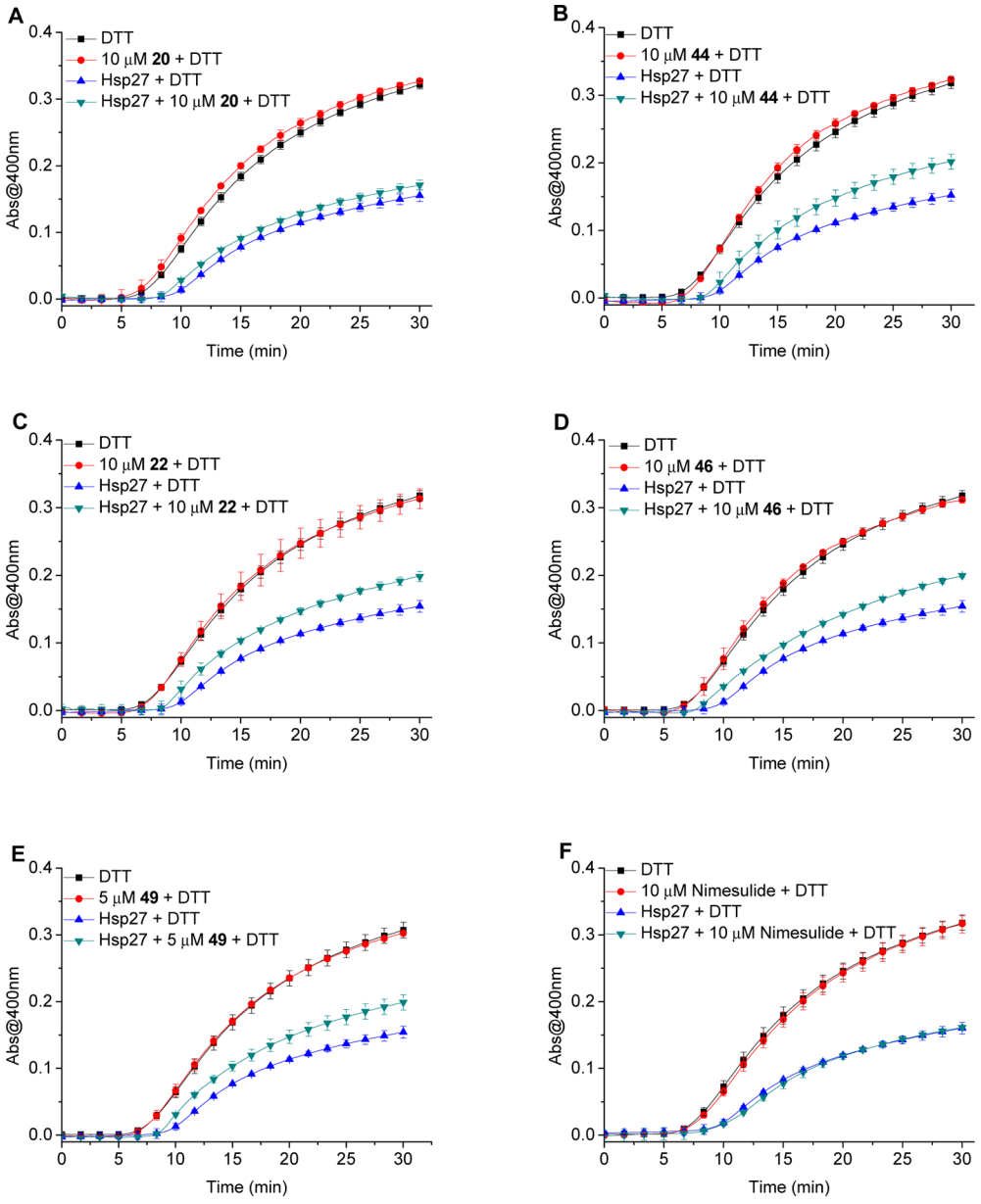

Figure 4. Hsp27 chaperone activity for the protection of DTT induced insulin aggregation in the presence of different concentrations of compounds **20**, **22**, **44**, **46**, **49** and nimesulide. The kinetics of the DTT reduction-induced insulin aggregation was monitored in the absence of Hsp27 or in the presence of Hsp27 without or with compounds in triplicate.

activity compared to compound **46** as well. **22** and **46** at 1 μM inhibited tubulin polymerization by 64% and 34%, respectively. The results suggest that the structural modification by substitution of 2,5-dimethylbenzyl group in compounds **44** and **46** with 2,5-dimethoxybenzyl group obviously increased their tubulin inhibitory activity. Moreover, 4-methoxybenzoxyamides at 100 nM showed more potent tubulin inhibition than the corresponding 4-iodobenzoxyamides, which is demonstrated by **20** versus **22** and **44** versus **46**. The tubulin inhibitory activities of compounds **20** and **22** match the cell cycle arrest activities very well. To summarize the tubulin inhibitory activity of the series of compounds, the earlier version lead compound and the first generation compound **49** (JCC76)[27,28] was also examined, and it slightly inhibited tubulin polymerization by 5% at 5 μM. The very first lead compound cyclooxygenase 2 (COX-2) inhibitor nimesulide[28] showed about 14% tubulin inhibition at 100 μM (Figure 3). This suggests that along the lead optimization, the tubulin targeting effects of the compounds have significantly improved.

2.4. Hsp27 Targeting Effect Investigation. Although the lead compound **48** binds to Hsp27 and tubulin, it is still unclear if the compound affects Hsp27 chaperone activity.[24] It is well documented that Hsp27 plays an important role in the prevention of cell apoptosis and effectively prevents protein aggregation.[8,13] The cellular protective functions of Hsp27 in the apoptotic pathway are regulated by its chaperone activity, and this activity contributes to the protection of cells from stress stimuli.[14] Therefore, we examined how our new derivatives and previous lead compounds regulate Hsp27 chaperone function in this study. Insulin is often used as a model substrate protein to evaluate the chaperone activity of small heat shock proteins. Dithiothreitol (DTT) reduction of insulin can induce its B chain to aggregate. However in the presence of Hsp27, the aggregation of insulin B chain can be

dx.doi.org/10.1021/jm4004736 | J. Med. Chem. 2013, 56, 5306−5320

attenuated or even completely prevented because of the formation of stable complexes between Hsp27 and the unfolded B chain.[29−31] The capabilities of our compounds to modulate the in vitro chaperone function of Hsp27 were evaluated by monitoring the DTT-induced insulin aggregation in the presence of Hsp27, with or without our compounds. In the in vitro chaperone activity assays, Hsp27 exhibited strong potency against DTT-induced insulin aggregation, which was consistent with the results of other investigations.[29−31] Our compounds showed inhibitory activity against Hsp27 chaperone activity in the insulin aggregation assay (Figure 4). More specifically, compound **22** at 10 μM significantly inhibited Hsp27 functions by 27%. However, compound **20** only slightly inhibited Hsp27 by 9% at 10 μM. The second generation compounds **44** and **46** exhibited similar Hsp27 inhibition. Compound **44** at 10 μM significantly inhibited Hsp27 chaperone activity by 30%. And compound **46** at 10 μM inhibited Hsp27 function by 28%. The results suggest that the structural modification dissected the tubulin and Hsp27 inhibition on some of the third generation compounds. Compound **20** showed strong tubulin inhibition but weak Hsp27 inhibition. The second-generation compounds **44** and **46** showed similar Hsp27 inhibition compared to the third generation compound **22** but exhibited relatively weaker tubulin inhibition. The compounds were much less active than third generation compounds in the cell proliferation assay. At 5 μM, first generation compound **49** showed strong Hsp27 inhibition by 29% and minimal tubulin inhibitory activity, which led to the lower cytotoxicity with an IC_{50} of 3.17 μM. In fact, compound **49** was the most potent Hsp27 inhibitor within the study and showed selective cytotoxicity to human epidermal growth factor receptor 2 (Her2) overexpressed breast cancer cells in a previous investigation,[32] which might be related to the Hsp27 and Her2 pathway interaction.[33,34] The parental compound nimesulide did not show any Hsp27 inhibitory activity at 10 μM. Moreover, all these compounds were evaluated in this assay in the absence of Hsp27 and the results demonstrated that the compounds exhibited no or minimal direct chemical chaperone activity on DTT-induced insulin aggregation.

Subsequently, we examined how the third generation compounds regulated Hsp27 in cancer cells. We first checked the levels of phosphorylated Hsp27 (pHsp27) and total Hsp27 in SKBR-3 breast cancer cells after a 24 h treatment with **20** and **22**. pHsp27 levels were significantly increased by both compounds at concentrations close to their IC_{50} values to inhibit cell growth (Figure 5). Since compound **20** did not show significant Hsp27 inhibition at 10 μM in the enzymatic assay but still stimulated cellular pHsp27, we speculate that the increased pHsp27 is not due to the Hsp27 direct targeting effect. The tubulin inhibition of these compounds might be responsible for the pHsp27 up-regulation, which has been demonstrated by other tubulin inhibitors such as vinblastine and paclitaxel.[35] Cells activate pHsp27 as a defending mechanism after being stressed by tubulin inhibitors. The results suggest that compound **22** did not directly change Hsp27 total protein, and the up-regulated Hsp27 phosphorylation was due to the tubulin effect, even the compound inhibited Hsp27 chaperone activity. Hsp27 has chaperone activity and can stabilize its client proteins. As an Hsp27 binder, compound **22** might affect the cellular Hsp27 chaperone function and decrease the stability of the Hsp27 client proteins. We checked several representative proteins including Her2,[18]

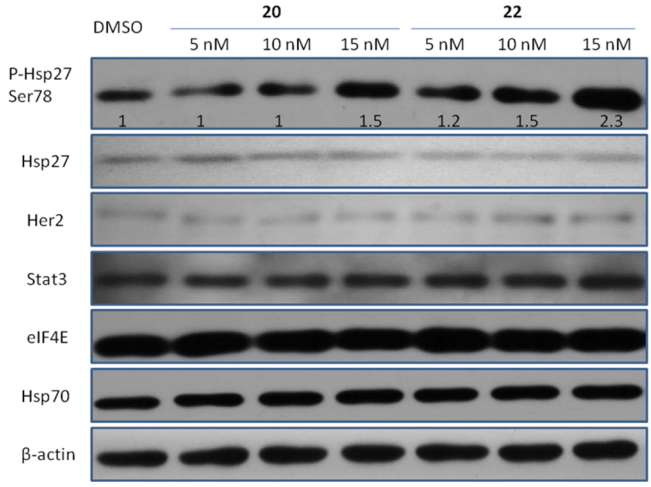

Figure 5. Effect of compounds **20** and **22** on Hsp27 and several Hsp27 interactive proteins. SKBR-3 cells were treated with DMSO and compounds **20** and **22** for 24 h. Levels of pHsp27, Hsp27, Her2, Stat3, eIF4E, and Hsp70 were analyzed by Western blot of cell extracts with specific antibodies as described in Experimental Section. The bands for pHsp27 were quantified using ImageJ (NIH) and normalized to β-actin.

eukaryotic translation initiation factor 4E (eIF4E),[36] signal transducer and activator of transcription 3 (Stat3),[37] and 70 kDa heat shock protein (Hsp70),[38] which have been reported to interact with Hsp27. These proteins in SKBR-3 cells were determined via Western blot after the treatment with compounds **20** and **22**. The results indicated that the protein levels of Her2, eIF4E, Stat3, and Hsp70 remained nearly constant after the treatment, which suggests that our Hsp27 inhibitor did not affect the stability of Her2, eIF4E, Stat3, and Hsp70 in SKBR-3 cells. As a general chaperone protein, Hsp27 has many client proteins. It is very desirable to identify some of these proteins that are sensitive to Hsp27 small molecule inhibitors, which can be used as a biomarker for Hsp27 inhibitor characterization. Although we did not find such a biomarker within the four Hsp27 client proteins, further investigation will be executed when more Hsp27 client proteins are discovered.

So far, our dual tubulin and Hsp27 inhibitor development has gone through three major stages, which can be represented by the three generations of compounds (Figure 6). The first generation compound **49** (JCC76)[27,28] was developed based on the COX-2 inhibitor nimesulide and showed promising antiproliferative activity with an IC_{50} of 3.17 μM. Examination of **49** with tubulin and Hsp27 enzymatic assays revealed that the compound mainly inhibited Hsp27 activity. The parental compound nimesulide did not show significant activities in the tubulin and Hsp27 assays. Apparently, the structural modification based on nimesulide as a platform led to novel tubulin and Hsp27 dual inhibitor, which was totally independent of COX-2 activity. The further ligand-based optimization of compound **49** resulted in the second generation of derivatives including compounds **43**−**48**, which exhibited significantly improved cell growth inhibitory activity with IC_{50} of 0.1−0.2 μM.[25] The mechanism investigation demonstrated that the tubulin inhibition of compounds **44** and **46** was greatly improved. And the Hsp27 chaperone inhibition of **44** and **46** was decreased compared to **49**. In the current study, we further optimized the second generation of

dx.doi.org/10.1021/jm4004736 | J. Med. Chem. 2013, 56, 5306−5320

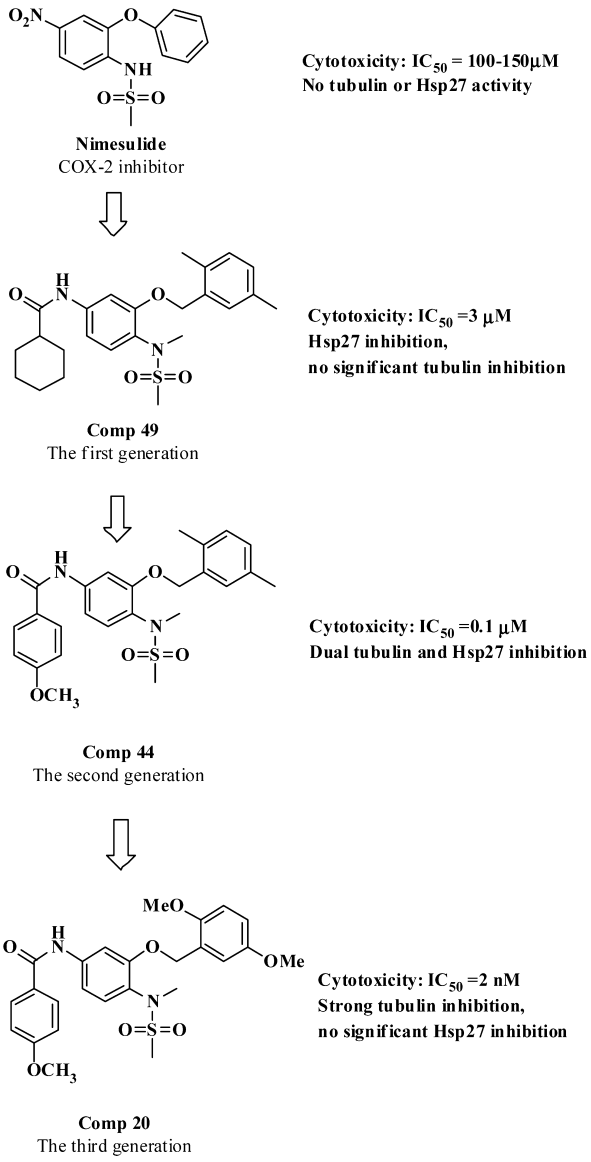

Figure 6. Development of potent anticancer agents from COX-2 inhibitor nimesulide to compound **20**.

compounds and generated a series of extremely potent antiproliferative agents such as compounds **20** and **22** with IC_{50} of around 2 nM. The mechanism investigation revealed that the Hsp27 effect of compound **20** was almost diminished, which was accompanied by a dramatic increase in tubulin inhibition. However, compound **22** still retained similar Hsp27 inhibition and also obtained a significant increase in tubulin inhibition compared to its second generation analogue **46**. The dual targeting effects of compound **22** have made it the most active analogue in the current study. Unexpectedly, we successfully dissected the two activities on compound **20**.

2.5. Broad Anticancer Activities. Because of the higher cytotoxic characteristics of compounds **20** and **22** on SKBR-3 breast cancer cells, they were submitted to the Developmental Therapeutic Program at the National Cancer Institute for screening against 60 human cancer cell lines, representing leukemia, melanoma, and cancers of the lung, colon, CNS, ovary, renal, prostate, and breast. Sixty cell lines from each class of cancer cells were incubated for 48 h with compounds **20** and **22** of various concentrations ranging from 10 nM to 100 μM. GI_{50} (50% of growth inhibition), TGI (total growth inhibition), and LC_{50} (loss of 50% of the initial cell protein) were calculated and summarized (Supporting Information). Compounds **20** and **22** exhibited extensive anticancer activity by inducing 50% of growth inhibition of most cell lines at concentrations less than 10 nM. These data (Supporting Information) clearly demonstrate the in vitro efficacy of compounds **20** and **22**.

2.6. Investigation of the Combination Treatment with Hsp27 Inhibitor and Tubulin Inhibitor. Hsp27 modulators exhibited synergistic anticancer effect when they were combined with other chemotherapeutic agents.[4,16,21,22,39,40] On the basis of our mechanism investigation, the first generation compound **49** mainly targeted Hsp27 chaperone activity, and the third generation compound **20** was almost a pure tubulin inhibitor. It would be interesting to see if the combination of compounds **49** and **20** could show an additive effect to inhibit cancer cell proliferation. Compound **49** at 0.5, 1.0, and 2.0 μM significantly shifted the cell growth inhibition curve of compound **20** to the left, suggesting that compound **49** could promote the activity of compound **20** (Figure 7A) despite that compound **49** alone did not show any cytotoxicity at 0.5 and 1.0 μM (Figure 7B). Similarly, when we combined compound **20** at 1.0, 1.5, and 2.0 nM with various concentrations of compound **49**, the cell growth inhibition curve of **49** was shifted to the left, suggesting that compound **20** could potentiate the activity of **49** as well (Figure 7B). The results further demonstrated the synergistic anticancer mechanism of the first generation compound **49** and third generation compound **20**.

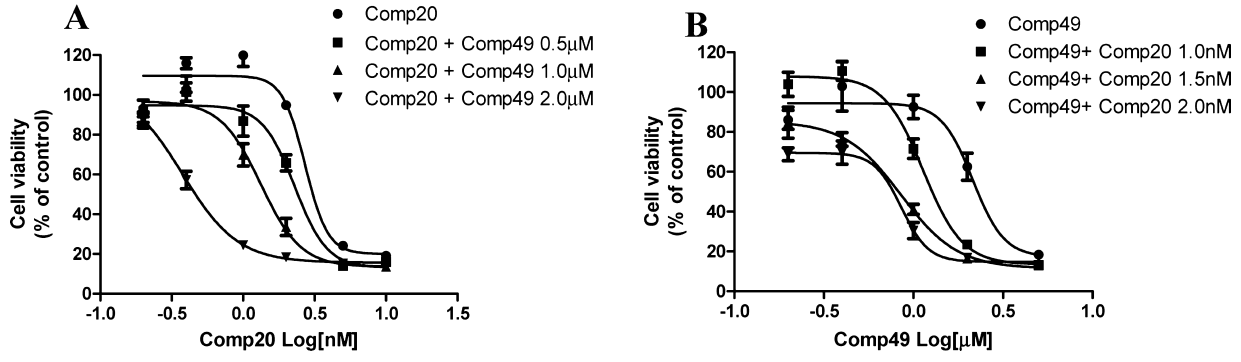

Figure 7. First generation compound **49** and third generation compound **20** combination treatment on SKBR-3 breast cancer cell proliferation. (A) Compound **49** at 0.5, 1.0, and 2.0 μM shifted compound **20** cell proliferation inhibition curve to the left, suggesting the additive effect of the two compounds. (B) Compound **20** at 1, 1.5, and 2.0 nM shifted compound **49** cell proliferation inhibition curve to the left.

dx.doi.org/10.1021/jm4004736 | J. Med. Chem. 2013, 56, 5306−5320

3. CONCLUSION

We developed a series of potent anticancer agents with IC_{50} values at subnanomolar levels to inhibit the proliferation of various cancer cell lines. Several new compounds such as **19**–**22** are 57- to 230-fold more active than previous lead compound **48**. The significantly increased anticancer activity is mainly attributed to the structural modification by substitution of 2,5-dimethylbenzyl moiety in the lead compound with a 2,5-dimethoxybenzyl group.

These compounds mainly targeted tubulin polymerization to inhibit cancer cell proliferation. Their Hsp27 inhibition also contributed to their significant anticancer activity. The conclusion is based on the results of tubulin and Hsp27 enzymatic assays. In the tubulin polymerization inhibition and Hsp27 chaperone activity assays, two pairs of compounds, **20** versus **44** and **22** versus **46**, were evaluated. The only structural difference in each pair of compounds is the 2,5-dimethoxybenzyl moiety in the former and the 2,5-dimethylbenzyl moiety in the latter compounds. The results indicated that the new analogues **20** and **22** exhibited much better tubulin inhibition compared to **44** and **46**, which led to the dramatic increase in their anticancer activity. Unexpectedly, the structural modification significantly decreased the Hsp27 inhibition of compound **20**. We fortunately dissected the dual anticancer activities on one of the third generation of compounds. Compound **22** inhibited Hsp27 at a similar level as **46**, and the dual targeting effect made this compound the most potent one in this series of new derivatives, even if it was less active than compound **20** to inhibit tubulin polymerization. The combination of the 4-methoxylbenzamide moiety and the 2,5-dimethoxybenzyl moiety of compound **20** improved the tubulin inhibitory activity and decreased the Hsp27 chaperone function inhibition. The SAR summarized in the study is very important for further drug optimization to generate more potent and selective inhibitors. Particularly, potent Hsp27 inhibitors can provide a solution to solve the drug resistance issues of many chemotherapeutic agents[16,22,36] and have great clinical application potential. Future study will focus on discerning the structural fragments, which are important for Hsp27 effects, developing more selective and potent Hsp27 inhibitors, and investigating the consequence of Hsp27 modulation. The investigation of how Hsp27 inhibitors regulate Hsp27 oligomerization, its chaperone functions, and the activity/stability of its client proteins could provide important information to elucidate their anticancer mechanisms.

4. EXPERIMENTAL SECTION

4.1. Chemistry. Chemicals were commercially available and used as received without further purification unless otherwise noted. Moisture sensitive reactions were carried out under a dry argon atmosphere in flame-dried glassware. Solvents were distilled before use under argon. Thin-layer chromatography was performed on precoated silica gel F254 plates (Whatman). Silica gel column chromatography was performed using silica gel 60 Å (Merck, 230–400 mesh), and hexane/ethyl acetate was used as the elution solvent. Mass spectra were obtained on a Micromass quadrupole time-of-flight (QTOF) electrospray mass spectrometer at Cleveland State University MS facility center. All the NMR spectra were recorded on a Bruker 400 MHz instrument in either DMSO-d_6 or $CDCl_3$. Chemical shifts (δ) for ^{1}H NMR spectra are reported in parts per million to residual solvent protons. The purity of the final compounds was determined via HPLC (Beckman) analysis with different mobile phases (Supporting Information). All the final compounds exhibited purities above 95%. The chromatographic separation was performed on a C18 column (2.0 mm × 150 mm, 5 μm) from Phenomenex (Torrance, CA). Two mobile phases (H_2O/CH_3OH, H_2O/CH_3CN) were employed for isocratic elution with a flow rate of 0.2 mL/min. The injection volume was 20 μL, and the UV detector was set up at 256 and 290 nm.

Intermediate compounds **1a**–**e**, **2a**–**d**, **3a**–**d**, **3d**′, and **4a**–**d** were prepared according to the previously published procedures.[25]

Trifluoromethanesulfonamides **2e**–**f** were prepared from aryl-substituted 2-amino-5-nitrophenols **1d**–**e** according to a modified procedure. NaH (95% powder, 0.211g, 8.81 mmol) was added to a solution of aryl-substituted 2-amino-5-nitrophenol **1d**–**e** (3.67 mmol) in anhydrous Et_2O (70 mL) at room temperature. After being stirred for 20 min, the mixture was cooled to 0 °C and Tf_2O (1.24 g, 4.4 mmol) was slowly added. The resulting mixture was continuously stirred for 1 h at 0–5 °C. Water (15 mL) was added to quench the reaction. Ether was evaporated under vacuum, and then 3 N HCl (4 mL) was added to acidify the residue. The intermediates **2e**–**f** precipitated as a yellow solid. It was collected by filtration, washed with water, dried in air, and then used for the next reaction directly. According to the same procedures used for preparation of intermediates **4a**–**d**, **2e**–**f** was subjected to N-methylation to afford **3e**–**f** followed by reduction of nitro group to give **4e**–**f**.

*N-Methyl-N-[2-(2,5-dimethoxybenzyloxy)-4-nitrophenyl]-trifluoromethanesulfonamide (**3e**).* Yellow solid, 59% yield for the two steps of sulfonylamidation and N-methylation; ^{1}H NMR (400 MHz, $CDCl_3$) δ 8.038 (1H, d, J = 2.4 Hz), 7.849 (1H, dd, J = 2.4, 8.8 Hz), 7.493 (1H, d, J = 8.8 Hz), 7.036 (1H, s), 6.876 (2H, m), 5.293 (2H, s), 3.889 (3H, s), 3.775 (3H, s), 3.414 (3H, s).

*N-Methyl-N-[2-(2,5-dimethylbenzyloxy)-4-nitrophenyl]-trifluoromethanesulfonamide (**3f**).* Yellow solid, 78% yield for the two steps of sulfonylamidation and N-methylation; ^{1}H NMR (400 MHz, $CDCl_3$) δ 7.974 (1H, d, J = 2.4 Hz), 7.895 (1H, dd, J = 2.4, 8.4 Hz), 7.531 (1H, d, J = 8.4 Hz), 7.242 (1H, s), 7.143 (2H, m), 5.195 (2H, s), 3.365 (3H, s), 2.374 (3H, s), 2.345 (3H, s).

*N-[4-Amino-2-(2,5-dimethoxybenzyloxy)phenyl]-N-methyltrifluoromethanesulfonamide (**4e**).* Pale white solid, 96% yield; ^{1}H NMR (400 MHz, $CDCl_3$) δ 7.115 (1H, s), 7.062 (1H, d, J = 8.4 Hz), 6.827 (2H, m), 6.315 (1H, d, J = 2.4 Hz), 6.217 (1H, dd, J = 2.4, 8.8 Hz), 5.101 (2H, s), 3.822 (3H, s), 3.817 (2H, br), 3.783 (3H, s), 3.359 (3H, s).

*N-[4-Amino-2-(2,5-dimethylbenzyloxy)phenyl]-N-methyltrifluoromethanesulfonamide (**4f**).* Pale white solid, 98% yield; ^{1}H NMR (400 MHz, $CDCl_3$) δ 7.257 (1H, s), 7.084 (3H, m), 6.319 (1H, d, J = 2.4 Hz), 6.234 (1H, dd, J = 2.4, 8.4 Hz), 5.006 (2H, s), 3.847 (2H, br), 3.312 (3H, s), 2.332 (3H, s), 2.315 (3H, s).

The final compounds **1**–**42** were prepared from the reaction of the corresponding substituted anilines (**4a**–**f** and **3d**′) with each arylcarbonyl chloride including 4-bromobenzoyl chloride, 4-methoxybenzoyl chloride, 3,4-dimethoxybenzoyl chloride, 4-iodobenzoyl chloride, 2-naphthoyl chloride, and piperonyloyl chloride.

*N-[3-(2,5-Dichlorobenzyloxy)-4-(methanesulfonylmethylamino)-phenyl]-4-bromobenzamide (**1**).* White solid, 65% yield; ^{1}H NMR (400 MHz, $CDCl_3$) δ 8.153 (1H, s), 7.795 (1H, s), 7.778 (2H, d, J = 8.4 Hz), 7.635 (2H, d, J = 8.4 Hz), 7.553 (1H, d, J = 2 Hz), 7.365 (1H, d, J = 8.4 Hz), 7.303 (2H, m), 6.946 (1H, dd, J = 2, 8.4 Hz), 5.086 (2H, s), 3.252 (3H, s), 2.878 (3H, s). ESI-MS calculated for $C_{22}H_{20}BrCl_2N_2O_4S$ $[M + H]^+$, 556.97; found, 556.94.

*N-[3-(2,5-Dichlorobenzyloxy)-4-(methanesulfonylmethylamino)-phenyl]-4-methoxybenzamide (**2**).* White solid, 70% yield; ^{1}H NMR (400 MHz, $CDCl_3$) δ 7.959 (1H, s), 7.919 (1H, d, J = 2 Hz), 7.860 (2H, d, J = 9.2 Hz), 7.550 (1H, d, J = 2.4 Hz), 7.311 (3H, m), 6.988 (2H, d, J = 8.8 Hz), 6.903 (1H, dd, J = 2.4, 8.4 Hz), 5.164 (2H, s), 3.884 (3H, s), 3.249 (3H, s), 2.850 (3H, s). ESI-MS calculated for $C_{23}H_{23}Cl_2N_2O_5S$ $[M + H]^+$, 509.07; found, 509.11.

*N-[3-(2,5-Dichlorobenzyloxy)-4-(methanesulfonylmethylamino)-phenyl]-3,4-dimethoxybenzamide (**3**).* White solid, 86% yield; ^{1}H NMR (400 MHz, $CDCl_3$) δ 8.047 (1H, s), 7.925 (1H, d, J = 2.4 Hz), 7.548 (1H, d, J = 2.4 Hz), 7.502 (1H, d, J = 2 Hz), 7.435 (1H, dd, J = 2, 8.4 Hz), 7.334 (3H, m), 6.911 (2H, m), 5.152 (2H, s), 3.960 (3H, s), 3.955 (3H, s), 3.250 (3H, s), 2.858 (3H, s). ESI-MS calculated for $C_{24}H_{25}Cl_2N_2O_6S$ $[M + H]^+$, 539.08; found, 539.12.

dx.doi.org/10.1021/jm4004736 | J. Med. Chem. 2013, 56, 5306–5320

*N-[3-(2,5-Dichlorobenzyloxy)-4-(methanesulfonylmethylamino)-phenyl]-4-iodobenzamide (**4**).* White solid, 85% yield; ^{1}H NMR (400 MHz, DMSO-d_6) δ 7.941 (2H, m), 7.773 (1H, d, J = 2.4 Hz), 7.745 (2H, m), 7.681 (1H, d, J = 2.4 Hz), 7.593 (1H, d, J = 8.4 Hz), 7.501 (1H, dd, J = 2.8, 8.4 Hz), 7.464 (1H, dd, J = 2.4, 8.4 Hz), 7.329 (1H, d, J = 8.4 Hz), 5.215 (2H, s), 3.139 (3H, s), 2.931 (3H, s). ESI-MS calculated for $C_{22}H_{20}Cl_2IN_2O_4S$ $[M + H]^+$, 604.96; found, 604.95.

*N-[3-(2,5-Dichlorobenzyloxy)-4-(methanesulfonylmethylamino)-phenyl]-2-naphthalenecarboxamide (**5**).* White solid, 98% yield; ^{1}H NMR (400 MHz, $CDCl_3$) δ 8.413 (1H, s), 8.264 (1H, s), 7.948 (5H, m), 7.579 (3H, m), 7.360 (2H, m), 7.291 (1H, dd, J = 2.8, 8.8 Hz), 6.988 (1H, dd, J = 2, 8.4 Hz), 5.164 (2H, s), 3.262 (3H, s), 2.861 (3H, s). ESI-MS calculated for $C_{26}H_{23}Cl_2N_2O_4S$ $[M + H]^+$, 529.08; found, 529.07.

*N-[3-(2,5-Dichlorobenzyloxy)-4-(methanesulfonylmethylamino)-phenyl]-1,3-benzodioxole-5-carboxamide (**6**).* White solid, 84% yield; ^{1}H NMR (400 MHz, $CDCl_3$) δ 7.953 (1H, s), 7.864 (1H, d, J = 2.4 Hz), 7.548 (1H, d, J = 2.4 Hz), 7.428 (1H, dd, J = 1.6, 8 Hz), 7.370 (2H, m), 7.311 (2H, m), 6.898 (2H, m), 6.067 (2H, s), 5.143 (2H, s), 3.247 (3H, s), 2.860 (3H, s). ESI-MS calculated for $C_{23}H_{21}Cl_2N_2O_6S$ $[M + H]^+$, 523.05; found, 523.09.

*N-[3-(n-Hexyloxy)-4-(methanesulfonylmethylamino)phenyl]-4-bromobenzamide (**7**).* White solid, 60% yield; ^{1}H NMR (400 MHz, $CDCl_3$) δ 8.042 (1H, s), 7.836 (1H, s), 7.766 (2H, d, J = 8.4 Hz), 7.644 (2H, d, J = 8.4 Hz), 7.277 (1H, d, J = 8 Hz), 6.755 (1H, d, J = 8 Hz), 4.060 (2H, t, J = 6.4 Hz), 3.269 (3H, s), 2.936 (3H, s), 1.817 (2H, m), 1.467 (2H, m), 1.349 (4H, m), 0.911 (3H, t, J = 6.8 Hz). ESI-MS calculated for $C_{21}H_{28}BrN_2O_4S$ $[M + H]^+$, 483.10; found, 483.13.

*N-[3-(n-Hexyloxy)-4-(methanesulfonylmethylamino)phenyl]-4-methoxybenzamide (**8**).* White solid, 58% yield; ^{1}H NMR (400 MHz, $CDCl_3$) δ 7.889 (2H, m), 7.850 (2H, d, J = 8.8 Hz), 7.303 (1H, d, J = 8.4 Hz), 6.990 (2H, d, J = 8.4 Hz), 6.742 (1H, dd, J = 2, 8.4 Hz), 4.076 (2H, t, J = 6.4 Hz), 3.885 (3H, s), 3.271 (3H, s), 2.931 (3H, s), 1.821 (2H, m), 1.472 (2H, m), 1.350 (4H, m), 0.911 (3H, t, J = 6.8 Hz). ESI-MS calculated for $C_{22}H_{31}N_2O_5S$ $[M + H]^+$, 435.20; found, 435.22.

*N-[3-(n-Hexyloxy)-4-(methanesulfonylmethylamino)phenyl]-3,4-dimethoxybenzamide (**9**).* White solid, 75% yield; ^{1}H NMR (400 MHz, $CDCl_3$) δ 7.914 (2H, m), 7.503 (1H, d, J = 2 Hz), 7.406 (1H, dd, J = 2, 8.4 Hz), 7.313 (1H, d, J = 8.4 Hz), 6.929 (1H, d, J = 8.4 Hz), 6.751 (1H, dd, J = 2.4, 8.4 Hz), 4.084 (2H, t, J = 6.8 Hz), 3.966 (3H, s), 3.961 (3H, s), 3.277 (3H, s), 2.937 (3H, s), 1.828 (2H, m), 1.476 (2H, m), 1.353 (4H, m), 0.913 (3H, t, J = 6.8 Hz). ESI-MS calculated for $C_{23}H_{33}N_2O_6S$ $[M + H]^+$, 465.21; found, 465.23.

*N-[3-(n-Hexyloxy)-4-(methanesulfonylmethylamino)phenyl]-4-iodobenzamide (**10**).* Yellowish solid, 36% yield; ^{1}H NMR (400 MHz, $CDCl_3$) δ 8.055 (1H, s), 7.851 (3H, m), 7.617 (2H, d, J = 8.4 Hz), 7.271 (1H, d, J = 8.4 Hz), 6.749 (1H, dd, J = 2.4, 8.4 Hz), 4.056 (2H, t, J = 6.4 Hz), 3.267 (3H, s), 2.933 (3H, s), 1.814 (2H, m), 1.467 (2H, m), 1.348 (4H, m), 0.911 (3H, t, J = 7.2 Hz). ESI-MS calculated for $C_{21}H_{28}IN_2O_4S$ $[M + H]^+$, 531.08; found, 531.13.

*N-[3-(n-Hexyloxy)-4-(methanesulfonylmethylamino)phenyl]-2-naphthalenecarboxamide (**11**).* White solid, 83% yield; ^{1}H NMR (400 MHz, $CDCl_3$) δ 8.412 (1H, s), 8.297 (1H, s), 7.950 (5H, m), 7.594 (2H, m), 7.296 (1H, d, J = 8.4 Hz), 6.822 (1H, dd, J = 2, 8.4 Hz), 4.066 (2H, t, J = 6.8 Hz), 3.274 (3H, s), 2.922 (3H, s), 1.801 (2H, m), 1.458 (2H, m), 1.332 (4H, m), 0.909 (3H, t, J = 6.8 Hz). ESI-MS calculated for $C_{25}H_{31}N_2O_4S$ $[M + H]^+$, 455.20; found, 455.23.

*N-[3-(n-Hexyloxy)-4-(methanesulfonylmethylamino)phenyl]-1,3-benzodioxole-5-carboxamide (**12**).* Yellowish solid, 76% yield; ^{1}H NMR (400 MHz, $CDCl_3$) δ 7.969 (1H, s), 7.839 (1H, d, J = 2.4 Hz), 7.425 (1H, dd, J = 2, 8.4 Hz), 7.370 (1H, d, J = 2 Hz), 7.269 (1H, d, J = 8.4 Hz), 6.884 (1H, d, J = 8 Hz), 6.735 (1H, dd, J = 2.4, 8.4 Hz), 6.065 (2H, s), 4.055 (2H, t, J = 6.8 Hz), 3.265 (3H, s), 2.934 (3H, s), 1.811 (2H, m), 1.464 (2H, m), 1.346 (4H, m), 0.909 (3H, t, J = 6.8 Hz). ESI-MS calculated for $C_{22}H_{29}N_2O_6S$ $[M + H]^+$, 449.17; found, 449.20.

*N-[3-(2-Methyl-5-trifluoromethylbenzyloxy)-4-(methanesulfonyl-methylamino)phenyl]-4-bromobenzamide (**13**).* White solid, 78% yield; ^{1}H NMR (400 MHz, $CDCl_3$) δ 8.026 (2H, m), 7.759 (2H, m), 7.704 (1H, s), 7.653 (2H, m), 7.548 (1H, d, J = 8 Hz), 7.365 (1H, d, J = 8 Hz), 7.330 (1H, d, J = 8.4 Hz), 6.835 (1H, dd, J = 2.4, 8.4 Hz), 5.160 (2H, s), 3.228 (3H, s), 2.783 (3H, s), 2.457 (3H, s). ESI-MS calculated for $C_{24}H_{23}BrF_3N_2O_4S$ $[M + H]^+$, 571.05; found, 571.04.

*N-[3-(2-Methyl-5-trifluoromethylbenzyloxy)-4-(methanesulfonyl-methylamino)phenyl]-4-methoxybenzamide (**14**).* White solid, 97% yield; ^{1}H NMR (400 MHz, $CDCl_3$) δ 8.081 (1H, d, J = 2.4 Hz), 7.959 (1H, s), 7.860 (2H, m), 7.702 (1H, s), 7.543 (1H, d, J = 8 Hz), 7.362 (1H, d, J = 8 Hz), 7.330 (1H, d, J = 8.8 Hz), 6.990 (2H, m), 6.815 (1H, dd, J = 2, 8.4 Hz), 5.163 (2H, s), 3.883 (3H, s), 3.224 (3H, s), 2.770 (3H, s), 2.455 (3H, s). ESI-MS calculated for $C_{25}H_{26}F_3N_2O_5S$ $[M + H]^+$, 523.15; found, 523.15.

*N-[3-(2-Methyl-5-trifluoromethylbenzyloxy)-4-(methanesulfonyl-methylamino)phenyl]-3,4-dimethoxybenzamide (**15**).* White solid, 91% yield; ^{1}H NMR (400 MHz, $CDCl_3$) δ 8.087 (1H, s), 8.032 (1H, s), 7.707 (1H, s), 7.534 (2H, m), 7.432 (1H, d, J = 8 Hz), 7.345 (2H, m), 6.922 (1H, d, J = 8 Hz), 6.826 (1H, d, J = 8.4 Hz), 5.161 (2H, s), 3.965 (3H, s), 3.955 (3H, s), 3.227 (3H, s), 2.775 (3H, s), 2.453 (3H, s). ESI-MS calculated for $C_{26}H_{28}F_3N_2O_6S$ $[M + H]^+$, 553.16; found, 553.15.

*N-[3-(2-Methyl-5-trifluoromethylbenzyloxy)-4-(methanesulfonyl-methylamino)phenyl]-4-iodobenzamide (**16**).* White solid, 87% yield; ^{1}H NMR (400 MHz, $CDCl_3$) δ 8.064 (1H, s), 8.018 (1H, d, J = 2.4 Hz), 7.855 (2H, d, J = 8.4 Hz), 7.703 (1H, s), 7.616 (2H, d, J = 8.8 Hz), 7.546 (1H, d, J = 8.4 Hz), 7.363 (1H, d, J = 7.6 Hz), 7.314 (1H, d, J = 8.4 Hz), 6.833 (1H, dd, J = 2.4, 8.4 Hz), 5.149 (2H, s), 3.225 (3H, s), 2.781 (3H, s), 2.451 (3H, s). ESI-MS calculated for $C_{24}H_{23}F_3IN_2O_4S$ $[M + H]^+$, 619.04; found, 619.02.

*N-[3-(2-Methyl-5-trifluoromethylbenzyloxy)-4-(methanesulfonyl-methylamino)phenyl]-2-naphthalenecarboxamide (**17**).* White solid, 97% yield; ^{1}H NMR (400 MHz, DMSO-d_6) δ 10.580 (1H, s), 8.592 (1H, s), 8.070 (4H, m), 7.925 (1H, s), 7.833 (1H, d, J = 2 Hz), 7.654 (3H, m), 7.506 (2H, m), 7.351 (1H, d, J = 8.4 Hz), 5.264 (2H, s), 3.146 (3H, s), 2.909 (3H, s), 2.470 (3H, s). ESI-MS calculated for $C_{28}H_{26}F_3N_2O_4S$ $[M + H]^+$, 543.16; found, 543.15.

*N-[3-(2-Methyl-5-trifluoromethylbenzyloxy)-4-(methanesulfonyl-methylamino)phenyl]-1,3-benzodioxole-5-carboxamide (**18**).* White solid, 84% yield; ^{1}H NMR (400 MHz, $CDCl_3$) δ 8.032 (1H, s), 7.943 (1H, s), 7.701 (1H, s), 7.542 (1H, d, J = 8 Hz), 7.371 (4H, m), 6.888 (1H, d, J = 8 Hz), 6.812 (1H, d, J = 8 Hz), 6.065 (2H, s), 5.153 (2H, s), 3.223 (3H, s), 2.780 (3H, s), 2.453 (3H, s). ESI-MS calculated for $C_{25}H_{24}F_3N_2O_6S$ $[M + H]^+$, 537.13; found, 537.17.

*N-[3-(2,5-Dimethoxybenzyloxy)-4-(methanesulfonyl-methylamino)phenyl]-4-bromobenzamide (**19**).* White solid, 91% yield; ^{1}H NMR (400 MHz, $CDCl_3$) δ 7.933 (1H, s), 7.875 (1H, d, J = 2 Hz), 7.759 (2H, m), 7.647 (2H, m), 7.327 (1H, d, J = 8.4 Hz), 7.012 (1H, d, J = 2.8 Hz), 6.882 (1H, d, J = 2 Hz), 6.857 (2H, m), 5.130 (2H, s), 3.783 (3H, s), 3.779 (3H, s), 3.234 (3H, s), 2.816 (3H, s). ESI-MS calculated for $C_{24}H_{26}BrN_2O_6S$ $[M + H]^+$, 549.07; found, 549.12.

*N-[3-(2,5-Dimethoxybenzyloxy)-4-(methanesulfonyl-methylamino)phenyl]-4-methoxybenzamide (**20**).* White solid, 60% yield; ^{1}H NMR (400 MHz, $CDCl_3$) δ 7.932 (1H, d, J = 2.4 Hz), 7.863 (3H, m), 7.327 (1H, d, J = 8.4 Hz), 7.004 (3H, m), 6.853 (3H, m), 5.138 (2H, s), 3.886 (3H, s), 3.782 (6H, s), 3.232 (3H, s), 2.807 (3H, s). ESI-MS calculated for $C_{25}H_{29}N_2O_7S$ $[M + H]^+$, 501.17; found, 501.21.

*N-[3-(2,5-Dimethoxybenzyloxy)-4-(methanesulfonyl-methylamino)phenyl]-3,4-dimethoxybenzamide (**21**).* White solid, 80% yield; ^{1}H NMR (400 MHz, $CDCl_3$) δ 7.942 (1H, d, J = 2.4 Hz), 7.925 (1H, s), 7.504 (1H, d, J = 2 Hz), 7.411 (1H, dd, J = 2, 8.4 Hz), 7.332 (1H, d, J = 8.4 Hz), 7.016 (1H, d, J = 2.4 Hz), 6.928 (1H, d, J = 8.4 Hz), 6.861 (3H, m), 5.138 (2H, s), 3.968 (3H, s), 3.961 (3H, s), 3.783 (3H, s), 3.781 (3H, s), 3.236 (3H, s), 2.810 (3H, s). ESI-MS calculated for $C_{26}H_{31}N_2O_8S$ $[M + H]^+$, 531.18; found, 531.23.

*N-[3-(2,5-Dimethoxybenzyloxy)-4-(methanesulfonyl-methylamino)phenyl]-4-iodobenzamide (**22**).* White solid, 62% yield; ^{1}H NMR (400 MHz, $CDCl_3$) δ 7.940 (1H, s), 7.872 (3H, m), 7.608 (2H, m), 7.323 (1H, d, J = 8.4 Hz), 7.011 (1H, d, J = 2.8 Hz), 6.879 (1H, d, J = 2.4 Hz), 6.854 (2H, m), 5.127 (2H, s), 3.782 (3H, s), 3.778 (3H, s), 3.232 (3H, s), 2,814 (3H, s). ESI-MS calculated for $C_{24}H_{26}IN_2O_6S$ $[M + H]^+$, 597.06; found, 597.11.

*N-[3-(2,5-Dimethoxybenzyloxy)-4-(methanesulfonyl-methylamino)phenyl]-2-naphthalenecarboxamide (**23**).* White solid, 83% yield; ^{1}H NMR (400 MHz, $CDCl_3$) δ 8.402 (1H, s), 8.153 (1H, s), 7.947 (5H, m), 7.607 (2H, m), 7.355 (1H, d, J = 8.4 Hz), 7.028 (1H, d, J = 2.8 Hz), 6.940 (1H, dd, J = 2.4, 8.4 Hz), 6.855 (2H, m), 5.159 (2H, s), 3.786 (3H, s), 3.782 (3H, s), 3.248 (3H, s), 2.818 (3H, s). ESI-MS calculated for $C_{28}H_{29}N_2O_6S$ $[M + H]^+$, 521.17; found, 521.22.

*N-[3-(2,5-Dimethoxybenzyloxy)-4-(methanesulfonyl-methylamino)phenyl]-1,3-benzodioxole-5-carboxamide (**24**).* White solid, 66% yield; ^{1}H NMR (400 MHz, $CDCl_3$) δ 7.890 (1H, d, J = 2.4 Hz), 7.857 (1H, s), 7.412 (1H, dd, J = 1.6, 8 Hz), 7.368 (1H, d, J = 1.6 Hz), 7.318 (1H, d, J = 8.4 Hz), 7.012 (1H, d, J = 2.4 Hz), 6.891 (1H, d, J = 8 Hz), 6.852 (3H, m), 6.070 (2H, s), 5.128 (2H, s), 3.781 (6H, s), 3.230 (3H, s), 2.810 (3H, s). ESI-MS calculated for $C_{25}H_{27}N_2O_8S$ $[M + H]^+$, 515.15; found, 515.20.

*N-[3-(2,5-Dimethoxybenzyloxy)-4-(methanesulfonylamino)-phenyl]-4-bromobenzamide (**25**).* White solid, 80% yield; ^{1}H NMR (400 MHz, DMSO-d_6) δ 10.37 (1H, s), 9.02 (1H, s), 7.91(2H, d, J = 8.8 Hz), 7.76 (2H, d, J = 8.8 Hz), 7.68 (1H, 2.4 Hz), 7.41 (1H, dd, J = 2.4, 8.8 Hz), 7.28 (1H, d, J = 3.2 Hz), 7.22 (1H, d, J = 8.4 Hz), 6.98 (1H, d, J = 9.2 Hz), 6.88 (1H, dd, J = 3.2, 8.8 Hz), 5.08 (2H, s), 3.79 (3H, s), 3.73 (3H, s), 2.87 (3H, s). ESI-MS calculated for $C_{23}H_{24}BrN_2O_6S$ $[M + H]^+$, 535.05; found, 535.04.

*N-[3-(2,5-Dimethoxybenzyloxy)-4-(methanesulfonylamino)-phenyl]-4-methoxybenzamide (**26**).* White solid, 46% yield; ^{1}H NMR (400 MHz, DMSO- d_6) 10.159 (1H, s), 9.009 (1H, s), 7.966 (2H, d, J = 8.8 Hz), 7.705 (1H, d, J = 2.4 Hz), 7.415 (1H, dd, J = 2, 8.8 Hz), 7.292 (1H, d, J = 3.2 Hz), 7.208 (1H, d, J = 8.8 Hz), 7.073 (2H, d, J = 8.8 Hz), 6.981 (1H, d, J = 9.2 Hz), 6.883 (1H, dd, J = 3.2, 8.8 Hz), 5.077 (2H, s), 3.845 (3H, s), 3.789 (3H, s), 3.730 (3H, s), 2.863 (3H, s). ESI-MS calculated for $C_{24}H_{27}N_2O_7S$ $[M + H]^+$, 487.15; found, 487.14.

*N-[3-(2,5-Dimethoxybenzyloxy)-4-(methanesulfonylamino)-phenyl]-3,4-dimethoxybenzamide (**27**).* White solid, 36% yield; ^{1}H NMR (400 MHz, $CDCl_3$) δ 10.14 (1H, s), 8.99 (1H, s), 7.70 (1H, d, J = 2.4 Hz), 7.63 (1H, dd, J = 2, 8 Hz), 7.53 (1H, d, J = 2 Hz), 7.39 (1H, dd, J = 2.4, 8.4 Hz), 7.29 (1H, d, J = 2.8 Hz), 7.22 (1H, d, J = 8.8 Hz), 7.09 (1H, d, J = 8.4 Hz), 6.98 (1H, d, J = 8.4 Hz), 6.88 (1H, dd, J = 3.2, 8.8 Hz), 5.08 (2H, s), 3.85 (3H, s), 3.84 (3H, s), 3.79 (3H, s), 3.73 (3H, s), 2.87 (3H, s). ESI-MS calculated for $C_{25}H_{29}N_2O_8S$ $[M + H]^+$, 517.16; found, 517.16.

*N-[3-(2,5-Dimethoxybenzyloxy)-4-(methanesulfonylamino)-phenyl]-4-iodobenzamide (**28**).* White solid, 56% yield; ^{1}H NMR (400 MHz, DMSO-d_6) δ δ 10.355 (1H, s), 9.031 (1H, s), 7.933 (2H, d, J = 8.4 Hz), 7.749 (2H, d, J = 8.4 Hz), 7.678 (1H, d, J = 2.4 Hz), 7.411 (1H, dd, J = 2, 8.8 Hz), 7.282 (1H, d, J = 3.2 Hz), 7.223 (1H, d, J = 8.4 Hz), 6.979 (1H, d, J = 9.2 Hz), 6.881 (1H, dd, J = 2.8, 8.8 Hz), 5.077 (2H, s), 3.785 (3H, s), 3.726 (3H, s), 2.868 (3H, s). ESI-MS calculated for $C_{23}H_{24}IN_2O_6S$ $[M + H]^+$, 583.04; found, 583.02.

*N-[3-(2,5-Dimethoxybenzyloxy)-4-(methanesulfonylamino)-phenyl]-2-naphthalenecarboxamide (**29**).* White solid, 85% yield; ^{1}H NMR (400 MHz, $CDCl_3$) δ 10.50 (1H, s), 9.03 (1H, s), 8.59 (1H, s), 8.06 (4H, m), 7.75 (1H, d, J = 2 Hz), 7.65 (2H, m), 7.50 (1H, dd, J = 2, 8.4 Hz), 7.30 (1H, d, J = 3.2 Hz), 7.25 (1H, d, J = 8.8 Hz), 6.98 (1H, d, J = 8.8 Hz), 6.89 (1H, dd, J = 3.2, 8.8 Hz), 5.11 (2H, s), 3.80 (3H, s), 3.74 (3H, s), 2.88 (3H, s). ESI-MS calculated for $C_{27}H_{27}N_2O_6S$ $[M + H]^+$, 507.16; found, 507.15.

*N-[3-(2,5-Dimethoxybenzyloxy)-4-(methanesulfonylamino)-phenyl]-1,3-benzodioxole-5-carboxamide (**30**).* White solid, 46% yield; ^{1}H NMR (400 MHz, $CDCl_3$) δ 10.12 (1H, s), 9.00 (1H, s), 7.69 (1H, d, J = 2 Hz), 7.58 (1H, dd, J = 2, 8 Hz), 7.51 (1H, d, J = 1.6 Hz), 7.40 (1H, dd, J = 2.4, 8.8 Hz), 7.28 (1H, d, J = 3.2 Hz), 7.21 (1H, d, J = 8.8 Hz), 7.07 (1H, d, J = 8.4 Hz), 6.98 (1H, d, J = 9.2 Hz), 6.88 (1H, dd, J = 3.2, 9.2 Hz), 6.14 (2H, s), 5.07 (2H, s), 3,79 (3H, s), 3.73 (3H, s), 2.86 (3H, s). ESI-MS calculated for $C_{24}H_{25}N_2O_8S$ $[M + H]^+$, 501.13; found, 501.13.

*N-[3-(2,5-Dimethoxybenzyloxy)-4-(trifluoromethanesulfonyl-methylamino)phenyl]-4-bromobenzamide (**31**).* White solid, 73% yield; ^{1}H NMR (400 MHz, $CDCl_3$) δ 7.895 (1H, s), 7.724 (2H, d, J = 8.8 Hz), 7.662 (1H, s), 7.623 (2H, d, J = 8.4 Hz), 7.280 (1H, m), 7.110 (1H, s), 7.024 (1H, dd, J = 2, 8.4 Hz), 6.834 (1H, s), 6.831 (1H, s), 5.156 (2H, s), 3.810 (3H, s), 3.779 (3H, s), 3.388 (3H, s). ESI-MS calculated for $C_{24}H_{23}BrF_3N_2O_6S$ $[M + H]^+$, 603.04; found, 603.00.

*N-[3-(2,5-Dimethoxybenzyloxy)-4-(trifluoromethanesulfonyl-methylamino)phenyl]-4-methoxybenzamide (**32**).* White solid, 72% yield; ^{1}H NMR (400 MHz, $CDCl_3$) δ 7.831 (3H, m), 7.727 (1H, d, J = 2 Hz), 7.276 (1H, m), 7.129 (1H, s), 6.991 (3H, m), 6.837 (1H, s), 6.833 (1H, s), 5.183 (2H, s), 3.879 (3H, s), 3.815 (3H, s), 3.791 (3H, s).3.387 (3H, s). ESI-MS calculated for $C_{25}H_{26}F_3N_2O_7S$ $[M + H]^+$, 555.14; found, 555.13.

*N-[3-(2,5-Dimethoxybenzyloxy)-4-(trifluoromethanesulfonyl-methylamino)phenyl]-3,4-dimethoxybenzamide (**33**).* White solid, 61% yield; ^{1}H NMR (400 MHz, $CDCl_3$) δ 7.875 (1H, s), 7.750 (1H, d, J = 2 Hz), 7.485 (1H, d, J = 2 Hz), 7.385 (1H, dd, J = 2, 8.4 Hz), 7.283 (1H, d, J = 8.4 Hz), 7.131 (1H, s), 7.007 (1H, dd, J = 2, 8.4 Hz), 6.908 (1H, d, J = 8.4 Hz), 6.835 (2H, m), 5.184 (2H, s), 3.959 (3H, s), 3.952 (3H,s), 3.813 (3H, s), 3.794 (3H, s), 3.393 (3H, s). ESI-MS calculated for $C_{26}H_{28}F_3N_2O_8S$ $[M + H]^+$, 585.15; found, 585.13.

*N-[3-(2,5-Dimethoxybenzyloxy)-4-(trifluoromethanesulfonyl-methylamino)phenyl]-4-iodobenzamide (**34**).* White solid, 74% yield; ^{1}H NMR (400 MHz, $CDCl_3$) δ 7.910 (1H, s), 7.832 (2H, d, J = 8.4 Hz), 7.662 (1H, s), 7.570 (2H, d, J = 8.4 Hz), 7.273 (1H, d, J = 8.4 Hz), 7.107 (1H, s), 7.017 (1H, dd, J = 2, 8.4 Hz), 6.828 (2H, s), 5.148 (2H, s), 3.806 (3H, s), 3.777 (3H, s), 3.386 (3H, s). ESI-MS calculated for $C_{24}H_{23}F_3IN_2O_6S$ $[M + H]^+$, 651.03; found, 651.00.

*N-[3-(2,5-Dimethoxybenzyloxy)-4-(trifluoromethanesulfonyl-methylamino)phenyl]-2-naphthalenecarboxamide (**35**).* White solid, 92% yield; ^{1}H NMR (400 MHz, DMSO-d_6) δ 10.645 (1H, s), 8.604 (1H, s), 8.074 (4H,m), 7.829 (1H, s), 7.658 (2H, m), 7.583 (1H, d, J = 6.4 Hz), 7.389 (1H, d, J = 8.4 Hz), 7.127 (1H, d, J = 3.2 Hz), 7.012 (1H, d, J = 8.8 Hz), 6.918 (1H, dd, J = 3.2, 9.2 Hz), 5.151 (2H, s), 3.803 (3H, s), 3.727 (3H, s), 3.367 (3H, s). ESI-MS calculated for $C_{28}H_{26}F_3N_2O_6S$ $[M + H]^+$, 575.15; found, 575.13.

*N-[3-(2,5-Dimethoxybenzyloxy)-4-(trifluoromethanesulfonyl-methylamino)phenyl]-1,3-benzodioxole-5-carboxamide (**36**).* White solid, 69% yield; ^{1}H NMR (400 MHz, $CDCl_3$) δ 7.779 (1H, s), 7.694 (1H, d, J = 2 Hz), 7.389 (1H, dd, J = 1.6, 9.6 Hz), 7.348 (1H, d, J = 1.6 Hz), 7.279 (1H, d, J = 8.4 Hz), 7.122 (1H, s), 7.001 (1H, dd, J = 2, 8.4 Hz), 6.883 (1H, d, J = 8 Hz), 6.839 (1H, s), 6.835 (1H, s), 6.070 (2H, s), 5.183 (2H, s), 3.819 (3H, s), 3.792 (3H, s), 3.386 (3H, s). ESI-MS calculated for $C_{25}H_{24}F_3N_2O_8S$ $[M + H]^+$, 569.12; found, 569.10.

*N-[3-(2,5-Dimethylbenzyloxy)-4-(trifluoromethanesulfonyl-methylamino)phenyl]-4-bromobenzamide (**37**).* White solid, 81% yield; ^{1}H NMR (400 MHz, $CDCl_3$) δ 7.874 (1H, s), 7.835 (1H, s), 7.741 (2H, d, J = 8.8 Hz), 7.647 (2H, d, J = 8.8 Hz), 7.292 (2H, m), 7.098 (2H, m), 6.953 (1H, dd, J = 2.4, 8.4 Hz), 5.103 (2H, s), 3.344 (3H, s), 2.343 (3H, s), 2.335 (3H, s). ESI-MS calculated for $C_{24}H_{23}BrF_3N_2O_4S$ $[M + H]^+$, 571.05; found, 571.04.

*N-[3-(2,5-Dimethylbenzyloxy)-4-(trifluoromethanesulfonyl-methylamino)phenyl]-4-methoxybenzamide (**38**).* White solid, 66% yield; ^{1}H NMR (400 MHz, $CDCl_3$) δ 7.892 (1H, d, J = 2.4 Hz), 7.844 (3H, m), 7.291 (2H, m), 7.096 (2H, m), 6.994 (2H, m), 6.928 (1H, dd, J = 2, 8.4 Hz), 5.114 (2H, s), 3.887 (3H, s), 3.339 (3H, s), 2.347 (3H, s), 2.340 (3H, s). ESI-MS calculated for $C_{25}H_{26}F_3N_2O_5S$ $[M + H]^+$, 523.15; found, 523.14.

*N-[3-(2,5-Dimethylbenzyloxy)-4-(trifluoromethanesulfonyl-methylamino)phenyl]-3,4-dimethoxybenzamide (**39**).* White solid, 73% yield; ^{1}H NMR (400 MHz, $CDCl_3$) δ 7.894 (2H, m), 7.493 (1H, d, J = 2 Hz), 7.393 (1H, dd, J = 2, 8 Hz), 7.297 (2H, m), 7.096 (2H, m), 6.921 (2H, m), 5.113 (2H, s), 3.966 (3H, s), 3.959 (3H, s), 3.343 (3H, s), 2.341 (6H, s). ESI-MS calculated for $C_{26}H_{28}F_3N_2O_6S$ $[M + H]^+$, 553.16; found, 553.15.

*N-[3-(2,5-Dimethylbenzyloxy)-4-(trifluoromethanesulfonyl-methylamino)phenyl]-4-iodobenzamide (**40**).* White solid, 78% yield; ^{1}H NMR (400 MHz, $CDCl_3$) δ 7.891 (1H, s), 7.855 (2H, d, J = 8.4 Hz), 7.829 (1H, m), 7.587 (2H, d, J = 8.8 Hz), 7.293 (2H, m), 7.092 (2H, m), 6.949 (1H, dd, J = 2, 8.4 Hz), 5.092 (2H, s), 3.340 (3H, s), 2.335 (6H, s). ESI-MS calculated for $C_{24}H_{23}F_3IN_2O_4S$ $[M + H]^+$, 619.04; found, 619.01.

*N-[3-(2,5-Dimethylbenzyloxy)-4-(trifluoromethanesulfonyl-methylamino)phenyl]-2-naphthalenecarboxamide (**41**).* White

dx.doi.org/10.1021/jm4004736 | J. Med. Chem. 2013, 56, 5306−5320

solid, 60% yield; ^{1}H NMR (400 MHz, $CDCl_3$) δ 8.386 (1H, s), 8.098 (1H, s), 7.944 (5H, m), 7.606 (2H, m), 7.312 (2H, m), 7.097 (2H, m), 7.013 (1H, dd, J = 2, 8.4 Hz), 5.133 (2H, s), 3.356 (3H, s), 2.354 (3H, s), 2.338 (3H, s). ESI-MS calculated for $C_{28}H_{26}F_3N_2O_4S$ $[M + H]^+$, 543.16; found, 543.15.

*N-[3-(2,5-Dimethylbenzyloxy)-4-(trifluoromethanesulfonyl-methylamino)phenyl]-1,3-benzodioxole-5-carboxamide (**42**).* White solid, 66% yield; ^{1}H NMR (400 MHz, $CDCl_3$) δ 7.851 (1H, s), 7.802 (1H, s), 7.384 (2H, m), 7.298 (2H, m), 7.095 (2H, m), 6.902 (2H, m), 6.074 (2H, s), 5.105 (2H, s), 3.337 (3H, s), 2.344 (3H, s), 2.339 (3H, s). ESI-MS calculated for $C_{25}H_{24}F_3N_2O_6S$ $[M + H]^+$, 537.13; found, 537.12.

4.2. Biological Studies. *4.2.1. Cell Culture.* SKBR-3 cells were obtained from ATCC (Rockville, MD). The cells were maintained in RPMI 1640 medium supplemented with 10% fetal bovine serum (FBS), 2 mmol/L L-glutamine, 1 mmol/L sodium pyruvate, and 100 U/mL penicillin–streptomycin. FBS was heat inactivated for 30 min in a 56 °C water bath before use. Cell cultures were grown at 37 °C in a humidified atmosphere of 5% CO_2 in a VWR CO_2 incubator (Bridgeport NJ).

4.2.2. Cell Viability Analysis. The effects of the new derivatives on SKBR-3 cell viability were assessed using the 3-(4,5-dimethylthiazol-2-yl)-2,5-diphenyl-2*H*-tetrazolium bromide assay in six replicates. Cells were grown in RPMI 1640 medium in 96-well, flat-bottomed plates for 24 h and were exposed to various concentrations of the compounds dissolved in DMSO (final concentration of ≤0.1%) in medium for 48 h. Controls received DMSO vehicle at a concentration equal to that in drug-treated cells. The medium was removed, replaced by 200 μL of 0.5 mg/mL 3-(4,5-dimethylthiazol-2-yl)-2,5-diphenyl-2*H*-tetrazolium bromide in fresh medium, and cells were incubated in the CO_2 incubator at 37 °C for 2 h. Supernatants were removed from the wells, and the reduced 3-(4,5-dimethylthiazol-2-yl)-2,5-diphenyl-2*H*-tetrazolium bromide dye was solubilized in 200 μL/well DMSO. Absorbance at 570 nm was determined on a plate reader. Statistical and graphical information was determined using GraphPad Prism software (GraphPad Software Incorporated) and Microsoft Excel (Microsoft Corporation). IC_{50} values were determined using nonlinear regression analysis.

4.2.3. Cell Cycle Study. For all the assays, cells were treated for the indicated time. To analyze the cell cycle profile, treated cells were fixed overnight with 70% EtOH at −20 °C and stained with propidium iodide buffer [38 mM sodium citrate (pH 7.5), 69 μM propidium iodide, and 120 μg/mL RNase A]. Samples were mixed gently and incubated at room temperature in the dark for 15 min. Before the analysis by flow cytometry, 400 μL of binding buffer was immediately added to each sample. A total of 1.2×10^4 cells were acquired for each sample, and a maximum of 1×10^4 cells within the gated region were analyzed.

4.2.4. Tubulin Polymerization Assay. A mixture of 100 μL of microtubule-associated protein-rich tubulin (2 mg/mL, bovine brain, Cytoskeleton) in buffer containing 80 mM PIPES (pH 6.9), 2 mM $MgCl_2$, 0.5 mM EGTA, and 5% glycerol was mixed with DMSO (as control) or various concentrations of **20**, **22**, **44**, **46**, **49**, and nimesulide in DMSO and incubated at 37 °C. Then 1 μL of 100 mM GTP was added to the mixture to initiate the tubulin polymerization and the absorbance at 340 nm was monitored over 20 min using a Varian Cary 50 series spectrophotometer.

4.2.5. Hsp27 Chaperone Activity Assay. A mixture of 0.24 mg/mL human recombinant insulin (Life Technologies), 0.02 mg/mL Hsp27 (Cell Sciences), and compounds **20**, **22**, **44**, **46**, **49**, and nimesulide in 98 μL of sodium phosphate buffer, pH 7.4, was incubated at 37 °C for 5 min, whereupon 2 μL of 1 M DTT in the same assay buffer was added to initiate the insulin aggregation. The absorbance (A) at 400 nm was monitored over 30 min using a Varian Cary 50 series spectrophotometer. A mixture of 0.24 mg/mL insulin in the absence or presence of 0.02 mg/mL Hsp27 with DMSO was used as control. The Hsp27 inhibition potency (%) of compounds at 30 min were determined by

$$\frac{A_{(\text{Hsp27+compound+DTT})} - A_{(\text{Hsp27+DTT})}}{A_{\text{DTT}} - A_{(\text{Hsp27+DTT})}}$$

where $A_{(\text{Hsp27+compound+DTT})} - A_{(\text{Hsp27+DTT})}$ represents an increase of insulin aggregation level in the presence of Hsp27 with compounds compared to that in the presence of Hsp27 without compounds and $A_{\text{DTT}} - A_{(\text{Hsp27+DTT})}$ represents a decrease of insulin aggregation level caused by Hsp27.

4.2.6. Western Blot. SKBR-3 cells were treated with 5, 10, and 15 nM **20** and **22** for 24 h. The cells were lysed, briefly sonicated, and centrifuged at 12000*g* for 10 min. Then 30 μg of protein for each sample was boiled with 4× loading buffer for 5 min, electrophoresed on a 10% SDS–polyacrylamide gel, and transferred onto polyvinylidene difluoride (PVDF) membrane. For cleaved caspase 3 and PARP examination, 60 μg of protein was used. The membrane was blocked for 1 h with 5% nonfat milk in PBST and then incubated with specific primary antibody (Cell Signaling). After being washed, the membrane was incubated with horseradish-conjugated secondary antibody (Cell Signaling). The bands were visualized by chemiluminescence with ECL reagent (Thermo Scientific).

■ ASSOCIATED CONTENT

Ⓢ Supporting Information

Results from HPLC analysis for compounds **1**–**42** and the results of Developmental Therapeutic Program at the National Cancer Institute screening against 60 human tumor cell lines with compounds **20** and **22**. This material is available free of charge via the Internet at http://pubs.acs.org.

■ AUTHOR INFORMATION

Corresponding Author

*Phone: 216-687-9219. Fax: 216-687-9298. E-mail: B.su@csuohio.edu.

Notes

The authors declare no competing financial interest.

■ ACKNOWLEDGMENTS

This research was supported by a startup fund from Cleveland State University and also partially supported by Grant R15AI 103889 (B.S.), Center for Gene Regulation in Health and Disease of CSU, and National Science Foundation Major Research Instrumentation Grants CHE-0923398 and CHE-1126384. We thank the Developmental Therapeutic Program at the National Cancer Institute for screening the compounds against 60 human cancer cell lines.

■ ABBREVIATIONS USED

COX-2, cyclooxygenase 2; Hsp27, heat shock protein 27; MAPK, mitogen-activated protein kinase; ASO, antisense oligonucleotide; siRNA, small interfering RNA; SAR, structure–activity relationship; Her2, human epidermal growth factor receptor 2; eIF4E, eukaryotic translation initiation factor 4E; Stat3, signal transducer and activator of transcription 3; Hsp70, 70 kDa heat shock protein; PARP, poly ADP-ribose polymerase; FBS, fetal bovine serum; PVDF, polyvinylidene difluoride; DTT, dithiothreitol

■ REFERENCES

(1) Arts, H. J.; Hollema, H.; Lemstra, W.; Willemse, P. H.; De Vries, E. G.; Kampinga, H. H.; Van der Zee, A. G. Heat-shock-protein-27 (hsp27) expression in ovarian carcinoma: relation in response to chemotherapy and prognosis. *Int. J. Cancer* **1999**, *84*, 234–238.

(2) Garrido, C.; Mehlen, P.; Fromentin, A.; Hammann, A.; Assem, M.; Arrigo, A. P.; Chauffert, B. Inconstant association between 27-kDa

heat-shock protein (Hsp27) content and doxorubicin resistance in human colon cancer cells. The doxorubicin-protecting effect of Hsp27. *Eur. J. Biochem.* **1996**, *237*, 653−659.
(3) Hsu, H. S.; Lin, J. H.; Huang, W. C.; Hsu, T. W.; Su, K.; Chiou, S. H.; Tsai, Y. T.; Hung, S. C. Chemoresistance of lung cancer stemlike cells depends on activation of Hsp27. *Cancer* **2011**, *117*, 1516−1528.
(4) Kamada, M.; So, A.; Muramaki, M.; Rocchi, P.; Beraldi, E.; Gleave, M. Hsp27 knockdown using nucleotide-based therapies inhibit tumor growth and enhance chemotherapy in human bladder cancer cells. *Mol. Cancer Ther.* **2007**, *6*, 299−308.
(5) Garrido, C.; Brunet, M.; Didelot, C.; Zermati, Y.; Schmitt, E.; Kroemer, G. Heat shock proteins 27 and 70: anti-apoptotic proteins with tumorigenic properties. *Cell Cycle* **2006**, *5*, 2592−2601.
(6) Garrido, C.; Solary, E. A role of HSPs in apoptosis through "protein triage"? *Cell Death Differ.* **2003**, *10*, 619−620.
(7) Garrido, C.; Bruey, J. M.; Fromentin, A.; Hammann, A.; Arrigo, A. P.; Solary, E. HSP27 inhibits cytochrome *c*-dependent activation of procaspase-9. *FASEB J.* **1999**, *13*, 2061−2070.
(8) Concannon, C. G.; Gorman, A. M.; Samali, A. On the role of Hsp27 in regulating apoptosis. *Apoptosis* **2003**, *8*, 61−70.
(9) Bruey, J. M.; Ducasse, C.; Bonniaud, P.; Ravagnan, L.; Susin, S. A.; Diaz-Latoud, C.; Gurbuxani, S.; Arrigo, A. P.; Kroemer, G.; Solary, E.; Garrido, C. Hsp27 negatively regulates cell death by interacting with cytochrome c. *Nat. Cell Biol.* **2000**, *2*, 645−652.
(10) Kamradt, M. C.; Chen, F.; Sam, S.; Cryns, V. L. The small heat shock protein alpha B-crystallin negatively regulates apoptosis during myogenic differentiation by inhibiting caspase-3 activation. *J. Biol. Chem.* **2002**, *277*, 38731−38736.
(11) Pandey, P.; Farber, R.; Nakazawa, A.; Kumar, S.; Bharti, A.; Nalin, C.; Weichselbaum, R.; Kufe, D.; Kharbanda, S. Hsp27 functions as a negative regulator of cytochrome *c*-dependent activation of procaspase-3. *Oncogene* **2000**, *19*, 1975−1981.
(12) Bruey, J. M.; Paul, C.; Fromentin, A.; Hilpert, S.; Arrigo, A. P.; Solary, E.; Garrido, C. Differential regulation of HSP27 oligomerization in tumor cells grown in vitro and in vivo. *Oncogene* **2000**, *19*, 4855−4863.
(13) Garrido, C. Size matters: of the small HSP27 and its large oligomers. *Cell Death Differ.* **2002**, *9*, 483−485.
(14) Rogalla, T.; Ehrnsperger, M.; Preville, X.; Kotlyarov, A.; Lutsch, G.; Ducasse, C.; Paul, C.; Wieske, M.; Arrigo, A. P.; Buchner, J.; Gaestel, M. Regulation of Hsp27 oligomerization, chaperone function, and protective activity against oxidative stress/tumor necrosis factor alpha by phosphorylation. *J. Biol. Chem.* **1999**, *274*, 18947−18956.
(15) Gonzalez-Mejia, M. E.; Voss, O. H.; Murnan, E. J.; Doseff, A. I. Apigenin-induced apoptosis of leukemia cells is mediated by a bimodal and differentially regulated residue-specific phosphorylation of heat-shock protein-27. *Cell. Death Dis.* **2010**, *1*, e64.
(16) Baylot, V.; Andrieu, C.; Katsogiannou, M.; Taieb, D.; Garcia, S.; Giusiano, S.; Acunzo, J.; Iovanna, J.; Gleave, M.; Garrido, C.; Rocchi, P. OGX-427 inhibits tumor progression and enhances gemcitabine chemotherapy in pancreatic cancer. *Cell. Death Dis.* **2011**, *2*, e221.
(17) Elpek, G. O.; Karaveli, S.; Simsek, T.; Keles, N.; Aksoy, N. H. Expression of heat-shock proteins hsp27, hsp70 and hsp90 in malignant epithelial tumour of the ovaries. *APMIS* **2003**, *111*, 523−530.
(18) Kang, S. H.; Kang, K. W.; Kim, K. H.; Kwon, B.; Kim, S. K.; Lee, H. Y.; Kong, S. Y.; Lee, E. S.; Jang, S. G.; Yoo, B. C. Upregulated HSP27 in human breast cancer cells reduces herceptin susceptibility by increasing Her2 protein stability. *BMC Cancer* **2008**, *8*, No. 10.1186/1471-2407-8-286.
(19) Langer, R.; Ott, K.; Specht, K.; Becker, K.; Lordick, F.; Burian, M.; Herrmann, K.; Schrattenholz, A.; Cahill, M. A.; Schwaiger, M.; Hofler, H.; Wester, H. J. Protein expression profiling in esophageal adenocarcinoma patients indicates association of heat-shock protein 27 expression and chemotherapy response. *Clin. Cancer Res.* **2008**, *14*, 8279−8287.
(20) Sherman, M.; Multhoff, G. Heat shock proteins in cancer. *Ann. N.Y. Acad. Sci.* **2007**, *1113*, 192−201.
(21) Heinrich, J. C.; Tuukkanen, A.; Schroeder, M.; Fahrig, T.; Fahrig, R. RP101 (brivudine) binds to heat shock protein HSP27 (HSPB1) and enhances survival in animals and pancreatic cancer patients. *J. Cancer Res. Clin. Oncol.* **2011**, *137*, 1349−1361.
(22) Chauhan, D.; Li, G.; Shringarpure, R.; Podar, K.; Ohtake, Y.; Hideshima, T.; Anderson, K. C. Blockade of Hsp27 overcomes Bortezomib/proteasome inhibitor PS-341 resistance in lymphoma cells. *Cancer Res.* **2003**, *63*, 6174−6177.
(23) Zhong, B.; Lama, R.; Smith, K. M.; Xu, Y.; Su, B. Design and synthesis of a biotinylated probe of COX-2 inhibitor nimesulide analog JCC76. *Bioorg. Med. Chem. Lett.* **2011**, *21*, 5324−5327.
(24) Yi, X.; Zhong, B.; Smith, K. M.; Geldenhuys, W. J.; Feng, Y.; Pink, J. J.; Dowlati, A.; Xu, Y.; Zhou, A.; Su, B. Identification of a class of novel tubulin inhibitors. *J. Med. Chem.* **2012**, *55*, 3425−3435.
(25) Zhong, B.; Cai, X.; Chennamaneni, S.; Yi, X.; Liu, L.; Pink, J. J.; Dowlati, A.; Xu, Y.; Zhou, A.; Su, B. From COX-2 inhibitor nimesulide to potent anti-cancer agent: synthesis, in vitro, in vivo and pharmacokinetic evaluation. *Eur. J. Med. Chem.* **2012**, *47*, 432−444.
(26) Su, B.; Chen, S. Lead optimization of COX-2 inhibitor nimesulide analogs to overcome aromatase inhibitor resistance in breast cancer cells. *Bioorg. Med. Chem. Lett.* **2009**, *19*, 6733−6735.
(27) Zhong, B.; Cai, X.; Yi, X.; Zhou, A.; Chen, S.; Su, B. In vitro and in vivo effects of a cyclooxygenase-2 inhibitor nimesulide analog JCC76 in aromatase inhibitors-insensitive breast cancer cells. *J. Steroid Biochem. Mol. Biol.* **2011**, *126*, 10−18.
(28) Su, B.; Darby, M. V.; Brueggemeier, R. W. Synthesis and biological evaluation of novel sulfonanilide compounds as antiproliferative agents for breast cancer. *J. Comb. Chem.* **2008**, *10*, 475−483.
(29) Faiella, L.; Piaz, F. D.; Bisio, A.; Tosco, A.; De Tommasi, N. A chemical proteomics approach reveals Hsp27 as a target for proapoptotic clerodane diterpenes. *Mol. BioSyst.* **2012**, *8*, 2637−2644.
(30) Lelj-Garolla, B.; Mauk, A. G. Roles of the N- and C-terminal sequences in Hsp27 self-association and chaperone activity. *Protein Sci.* **2012**, *21*, 122−133.
(31) Lelj-Garolla, B.; Mauk, A. G. Self-association and chaperone activity of Hsp27 are thermally activated. *J. Biol. Chem.* **2006**, *281*, 8169−8174.
(32) Chen, B.; Su, B.; Chen, S. A COX-2 inhibitor nimesulide analog selectively induces apoptosis in Her2 overexpressing breast cancer cells via cytochrome c dependent mechanisms. *Biochem. Pharmacol.* **2009**, *77*, 1787−1794.
(33) Kang, S. H.; Kang, K. W.; Kim, K. H.; Kwon, B.; Kim, S. K.; Lee, H. Y.; Kong, S. Y.; Lee, E. S.; Jang, S. G.; Yoo, B. C. Upregulated HSP27 in human breast cancer cells reduces herceptin susceptibility by increasing Her2 protein stability. *BMC Cancer* **2008**, *8*, No. 10.1186/1471-2407-8-286.
(34) Zhang, D.; Tai, L. K.; Wong, L. L.; Chiu, L. L.; Sethi, S. K.; Koay, E. S. Proteomic study reveals that proteins involved in metabolic and detoxification pathways are highly expressed in HER-2/neu-positive breast cancer. *Mol. Cell. Proteomics* **2005**, *4*, 1686−1696.
(35) Casado, P.; Zuazua-Villar, P.; Prado, M. A.; Valle, E. D.; Iglesias, J. M.; Martinez-Campa, C.; Lazo, P. S.; Ramos, S. Characterization of HSP27 phosphorylation induced by microtubule interfering agents: implication of p38 signalling pathway. *Arch. Biochem. Biophys.* **2007**, *461*, 123−129.
(36) Andrieu, C.; Taieb, D.; Baylot, V.; Ettinger, S.; Soubeyran, P.; De-Thonel, A.; Nelson, C.; Garrido, C.; So, A.; Fazli, L.; Bladou, F.; Gleave, M.; Iovanna, J. L.; Rocchi, P. Heat shock protein 27 confers resistance to androgen ablation and chemotherapy in prostate cancer cells through eIF4E. *Oncogene* **2010**, *29*, 1883−1896.
(37) Gibert, B.; Eckel, B.; Fasquelle, L.; Moulinqq, M.; Bouhallier, F.; Gonin, V.; Mellier, G.; Simon, S.; Kretz-Remy, C.; Arrigo, A. P.; Diaz-Latoud, C. Knock down of heat shock protein 27 (HspB1) induces degradation of several putative client proteins. *PLoS One* **2012**, *7*, e29719.
(38) Kindas-Mugge, I.; Rieder, C.; Frohlich, I.; Micksche, M.; Trautinger, F. Characterization of proteins associated with heat shock protein hsp27 in the squamous cell carcinoma cell line A431. *Cell Biol. Int.* **2002**, *26*, 109−116.

(39) Sharma, A.; Upadhyay, A. K.; Bhat, M. K. Inhibition of Hsp27 and Hsp40 potentiates 5-fluorouracil and carboplatin mediated cell killing in hepatoma cells. *Cancer Biol. Ther.* **2009**, *8*, 2106−2113.
(40) Song, T. F.; Zhang, Z. F.; Liu, L.; Yang, T.; Jiang, J.; Li, P. Small interfering RNA-mediated silencing of heat shock protein 27 (HSP27) increases chemosensitivity to paclitaxel by increasing production of reactive oxygen species in human ovarian cancer cells (HO8910). *J. Int. Med. Res.* **2009**, *37*, 1375−1388.